

11-7-2015

# Investigations into the Regulation of the Redox Activity of Protein Disulfide Isomerase by Active Site-Flanking Lysines

Hyder Ali Khan  
*University of Windsor*

Follow this and additional works at: <http://scholar.uwindsor.ca/etd>

---

## Recommended Citation

Ali Khan, Hyder, "Investigations into the Regulation of the Redox Activity of Protein Disulfide Isomerase by Active Site-Flanking Lysines" (2015). *Electronic Theses and Dissertations*. Paper 5501.

This online database contains the full-text of PhD dissertations and Masters' theses of University of Windsor students from 1954 forward. These documents are made available for personal study and research purposes only, in accordance with the Canadian Copyright Act and the Creative Commons license—CC BY-NC-ND (Attribution, Non-Commercial, No Derivative Works). Under this license, works must always be attributed to the copyright holder (original author), cannot be used for any commercial purposes, and may not be altered. Any other use would require the permission of the copyright holder. Students may inquire about withdrawing their dissertation and/or thesis from this database. For additional inquiries, please contact the repository administrator via email ([scholarship@uwindsor.ca](mailto:scholarship@uwindsor.ca)) or by telephone at 519-253-3000ext. 3208.

**Investigations into the Regulation of the Redox Activity of Protein Disulfide  
Isomerase by Active Site-Flanking Lysines**

By

**Hyder Ali Khan**

A Thesis

Submitted to the Faculty of Graduate Studies  
through the Department of **Chemistry and Biochemistry**  
in Partial Fulfillment of the Requirements for  
the Degree of **Master of Science**  
at the University of Windsor

Windsor, Ontario, Canada

2015

© 2015 Hyder Ali Khan

**Investigations into the Regulation of the Redox Activity of Protein Disulfide  
Isomerase by Active Site-Flanking Lysines**

by

**Hyder Ali Khan**

APPROVED BY:

---

**J. Hudson**

Department of Biological Sciences

---

**P.O. Vacratsis**

Department of Chemistry and Biochemistry

---

**B. Mutus, Advisor**

Department of Chemistry and Biochemistry

July 27, 2015

## **DECLARATION OF ORIGINALITY**

I hereby certify that I am the sole author of this thesis and that no part of this thesis has been published or submitted for publication.

I certify that, to the best of my knowledge, my thesis does not infringe upon anyone's copyright nor violate any proprietary rights and that any ideas, techniques, quotations, or any other material from the work of other people included in my thesis, published or otherwise, are fully acknowledged in accordance with the standard referencing practices. Furthermore, to the extent that I have included copyrighted material that surpasses the bounds of fair dealing within the meaning of the Canada Copyright Act, I certify that I have obtained a written permission from the copyright owner(s) to include such material(s) in my thesis and have included copies of such copyright clearances to my appendix.

I declare that this is a true copy of my thesis, including any final revisions, as approved by my thesis committee and the Graduate Studies office, and that this thesis has not been submitted for a higher degree to any other University or Institution.

## ABSTRACT

Protein disulfide isomerase (PDI) is crucial in the redox of disulfide bonds, where it catalyzes reductase, oxidase, and isomerase activity. The active site motif for PDI is CXXC, which is found in the  $\alpha$  and  $\alpha'$  domain. PDI is mainly localized to the endoplasmic reticulum, where it plays a key role in the folding of new proteins through proper disulfide formation.

With new studies about the regulation of protein activity by lysine acetylation, our group wished investigate this post-translational modification on PDI. Flanking each active site motif of PDI is a lysine residue. These active site-flanking lysine residues were mutated individually and together to observe if any catalytic change occurred. Mutation of the lysine residue to glutamine, alanine, or glutamic acid resulted in a decrease in activity, indicating the importance of the lysine residue for optimal PDI activity. Acetylation of PDI was performed by acetic anhydride, where through mass spectrometry, PDI was observed to be partially acetylated. The catalytic efficiency of the acetylated wt-PDI was observed to decrease in comparison to un-acetylated PDI. Indicating that acetylation of PDI may be a possible regulator of PDI redox activity.

# DEDICATION

*This thesis is dedicated to my family and friends who supported me throughout my years in university*

## ACKNOWLEDGEMENTS

First and foremost, I would like to offer my heartfelt gratitude to my supervisor, Dr. Bulent Mutus, for the unwavering and steadfast support he has given me throughout the last two years of my masters. He has provided me with the opportunity to thrive as a researcher and was always there to push me further so that I may improve as a scientist. I would also like to thank the members of my supervisory committee, Dr. Panayiotis O. Vacratsis and Dr. John Hudson for their helpful ideas and suggestions.

None of this would have been possible without the assistance and support of the Department of Chemistry and Biochemistry. A special thanks is reserved for the collaborators who have taught me the importance of teamwork: Dr. Ananvoranich, for her expertise and skill in the preparations of the PDI mutants and Dr. Gauld and Wanlei Wei, for their computational contributions to my work. Another special thanks goes to Dr. Lee for her advice and support in my pursuit of future goals. I would like to thank Marlene Bezaire, Elizabeth Kickham, and Catherine Wilson for all their hard work which is seldom appreciated as it should be.

I truly appreciate all the support provided to me by my fellow lab members. To Adam, Artur, Bei, and Terence. It has truly been a pleasure to work with each of you every day and I am extremely grateful to have known you. The struggles and joys we shared together in lab are things I will never forget. I also took great pleasure in working with past and present undergraduate students; Cody, Kathy, Bianca, and Farzana, it was a humbling experience to be a part of your mentorship and growth as scientists. I would be remiss if I did not acknowledge the graduate student community at the Department of

Chemistry and Biochemistry as a whole, the feeling of comradery is something I will surely miss.

To the friends I have met in chemistry thank you for always being a source of enjoyment. I will always cherish our conversations during lunch. To Hi, Manar, Paul, and Phil for their unconditional friendship, the fun times we shared together, and for always being there to help me when I needed it.

Finally, I would like to thank my family for their love and support throughout my lifetime. I would have never made it this far without my parents, who always were there to provide guidance and wisdom. I would like to thank my sister and brothers, who gave me the roadmap on how to succeed in life.



## TABLE OF CONTENTS

DECLARATION OF ORIGINALITY .....	iii
ABSTRACT.....	iv
DEDICATION.....	v
ACKNOWLEDGEMENTS.....	vi
LIST OF TABLES.....	x
LIST OF FIGURES .....	xi
LIST OF ABBREVIATIONS/SYMBOLS.....	xvi
1 Introduction .....	1
1.1 Protein folding and the importance of disulfide bonds .....	1
1.2 Protein disulfide isomerase (PDI).....	2
1.2.1 Overview.....	2
1.2.2 Structural importance of PDI and the interplay with catalytic activity.....	4
1.2.3 PDI localization/protein interactions/physiological role .....	7
1.2.4 Catalytic activity assays for PDI.....	10
1.3 Acetyltransferases.....	11
1.4 Research objectives .....	15
2 Materials .....	16
2.1 Chemicals .....	16
2.2 Plasmids and primers.....	17
2.3 Equipment.....	18
3 Methods .....	20
3.1 Plasmid bacterial transformation .....	20
3.2 Bacterial mini prep .....	20
3.3 Site-directed mutagenesis.....	21
3.4 Protein purification .....	22
3.4.1 His-Tagged PDI protein purification.....	22

3.4.2	GST-Tagged protein purification.....	23
3.5	Di-Eosin-Glutathione Disulfide (Di-E-GSSG) synthesis.....	24
3.6	Quantification of Eosin Reduced Glutathione (EGSH).....	25
3.7	Determination of PDI concentration through burst kinetics .....	25
3.8	PDI kinetic assay.....	25
3.9	PDI acetylation.....	26
3.9.1	PDI Acetylation by acetyltransferase .....	26
3.9.2	PDI acetylation by acetic anhydride .....	26
3.10	Mass spectrometry analysis of PDI.....	27
3.11	Computational analysis .....	27
3.12	Statistical analysis.....	27
4	Results .....	29
4.1	Reductase activity of PDI and PDI-Mutants, at physiological pH .....	29
4.2	The effect of the active site lysine residues on the pH optima of the reductase activity of PDI .....	33
4.3	Reductase activity of wt-PDI and PDI mutants, at pH 6.5.....	35
4.4	Computational structural and pKa analysis of active site cysteine residues.....	39
4.5	Identification of acetylated active site lysine residues through mass spectrometry.....	41
4.6	Reductase activity of un-acetylated and acetylated PDI and PDI K-Q <i>aa'</i> .....	45
5	Discussion.....	51
5.1	The importance of active site-flanking lysine residues in the reductase activity of PDI	51
5.2	The possible regulation of PDI by lysine acetylation.....	54
6	Conclusion.....	60
	References .....	63
	Vita Auctoris.....	70

## LIST OF TABLES

Table 1. A summary of all site-directed mutations performed on PDI. All K-E mutations were performed by Cody Caba in completion of his Honours Thesis research project. ....	30
Table 2. Computationally estimated pKa's of active site cysteines in the <i>a</i> and <i>a'</i> domain. Wanlei Wei of Dr. Gauld's group performed the computational analysis of all the proteins (Li et al., 2005).....	40
Table 3. Sequences of acetylated peptides found in PDI through mass spectrometry. Lysine residues in red font indicate acetylated residue. Information taken from supplementary data of Pehar, M. et al. (2012). <i>Journal of Biological Chemistry</i> , 287(27).....	55

## LIST OF FIGURES

Figure 1. The 3 main redox reaction catalyzed by PDI: oxidation of thiols, reduction of disulfide, and isomerization of disulfide.....	3
Figure 2. Crystal Structure of Reduced and Oxidized PDI. (A) Reduced crystal structure of human PDI (PDB ID: 4EKZ). (B) Oxidized crystal structure of human PDI (PDB ID: 4EL1). (C) Schematic of PDI domains present in the crystal structure, as well as the two active site CXXC motifs. (Crystal structures created using Swiss PDBViewer). Image taken from Khan, H. A., & Mutus, B. (2014). <i>Frontiers in chemistry</i> , 2.....	5
Figure 3. The hypothesized regeneration of PDI by Ero1. The <i>a</i> domain of PDI oxidizes the substrate. The now reduced <i>a</i> domain is re-oxidized by the <i>a'</i> domain. The now reduced <i>a'</i> domain is re-oxidized by Ero1. The thiols of Ero1 are oxidized by O <sub>2</sub> ....	8
Figure 4. Fluorogenic Di-E-GSSG reductase assay. A) Structure of Di-E-GSSG. B) Reduction mechanism of Di-E-GSSG by PDI to produce the fluorescent EGSH. C) Fluorescent graph of reductase assay, where DTT demonstrates little increase in fluorescence. With the addition of PDI, fluorescence increases.....	12
Figure 5. Lysine acetylation by acetyltransferase and acetyl-CoA.....	13
Figure 6. Burst kinetics for wt-PDI and mutants. For each experiment, 10 μL of enzyme was reacted with 800 nM of Di-E-GSSG for 10 minutes. The linear regression was taken after the burst phase, where the y-intercept indicated the concentration of enzyme. All kinetics for K-E mutations (H, I, and J) were performed by Cody Caba as a part of his Honours Thesis research project.....	31

Figure 7. Initial rate vs. [Di-E-GSSG] plots for PDI and mutants. For each experiment the protein concentration was 20nM, and the initial rate was expressed as the amount of EGSH produced (nM/s). The assay was performed with 10µM of DTT in phosphate buffer (100mM phosphate pH 7.4, 0.1mM DTPA) and data was collected for 1 minute. The dashed lines represent the application of the best-fit kinetic parameters, obtained from the data, to the Michaelis-Menten equation. The error bars represent standard deviation, n=3. All kinetics for K-E mutations (G, H, and I) were performed by Cody Caba as a part of his Honours Thesis research project. .... 32

Figure 8. Michaelis-Menten kinetic parameters and catalytic efficiency ( $k_{cat}/K_M$ ) for wt-PDI and mutants at pH 7.4. The kinetic parameters and catalytic efficiency were estimated by utilizing a fit of the initial rate data of EGSH production by wt-PDI and the Lys variants by using the Solver function in MS Excel. Results are expressed as the mean with standard deviation, n=3. Significant differences ( $p<0.05$ ) are indicated by \*. All K-E mutation kinetics were performed by Cody Caba as a part of his Honours Thesis research project. .... 34

Figure 9. pH Titration curves of PDI and mutants. The concentration of wt-PDI was kept constant at 20nM and Di-E-GSSG was kept constant at 400nM. The change in pH occurred through the addition of NaOH. The rate was expressed as the amount of EGSH produced (nM/s). Results are expressed as the mean with standard deviation, n=3. All kinetics for K-E mutations (C) were performed by Cody Caba as a part of his Honours Thesis research project. .... 36

Figure 10. Initial rate vs. [Di-E-GSSG] plots for wt-PDI and mutants. For each experiment the protein concentration was 20nM, and the initial rate was expressed

as the amount of EGSH produced (nM/s). The assay was performed with 10 $\mu$ M of DTT in phosphate buffer (100mM phosphate pH 6.5, 0.1mM DTPA) and data was collected for 1 minute. The dashed lines represent the application of the best-fit kinetic parameters, obtained from the data, to the Michaelis-Menten equation. The error bars represent standard deviation, n=3. All kinetics for K-E mutations (G, H, and I) were performed by Cody Caba as a part of his Honours Thesis research project. .... 37

Figure 11. Michaelis-Menten kinetic parameters and catalytic efficiency ( $k_{cat}/K_M$ ) for wt-PDI and mutants. The kinetic parameters and catalytic efficiency were estimated from a fit of the initial rate data of EGSH production at pH 6.5 by wt-PDI and the Lys variants by using the Solver function in MS Excel. Results are expressed as the mean with standard deviation, n=3. Significant differences ( $p < 0.05$ ) are indicated by \*. All K-E mutation kinetics were performed by Cody Caba as a part of his Honours Thesis research project..... 38

Figure 12. Computational dynamics simulation of wt-PDI *a'* domain active site. Distances are provided in Angstroms. The atoms are represented by colours (yellow: sulfur, red: oxygen, blue: nitrogen, light grey: hydrogen, and dark grey: carbon). Wanlei Wei of Dr. Gauld's group performed the computational analysis of all the proteins..... 42

Figure 13. Computational dynamics simulation of acetylated wt-PDI *a'* domain active site. Distances are provided in Angstroms. The atoms are represented by colours (yellow: sulfur, red: oxygen, blue: nitrogen, light grey: hydrogen, and dark grey:

carbon). Wanlei Wei of Dr. Gauld's group performed the computational analysis of all the proteins..... 43

Figure 14. Mass fingerprint analysis of PDI Glu-C peptides. PDI digestion was performed overnight at room temperature using a 10:1 ratio of PDI to Glu-C. A) The mass fingerprint of PDI, where  $m/z$  1689 and 2459 corresponds to the active sites of PDI. B) The MS/MS of the  $m/z$  1689 parent ion corresponding to the  $a$  domain of PDI. C) The MS/MS of the  $m/z$  2459 parent ion corresponding to the  $a'$  domain of PDI..... 44

Figure 15. Mass fingerprint analysis of PDI reacted with acetyltransferase (PCAF). PDI was incubated with PCAF and acetyl-CoA for 2 hours at 32°C. PDI was the digested with Glu-C overnight at room temperature. Only the un-acetylated peptide fragments are observed in the mass fingerprint. .... 46

Figure 16. Mass fingerprint analysis of PDI reacted with acetic anhydride. PDI was incubated with acetic anhydride for 2 hours at 37°C. PDI was the digested with Glu-C overnight at room temperature. A) Un-acetylated peptide fragments are observed in the mass fingerprint. The  $a'$  active site domain is observed to be acetylated with a  $m/z$  2502. B) The MS/MS of the  $m/z$  2502 parent ion, which corresponds to the acetylated active site  $a'$  domain..... 47

Figure 17. Initial rate vs. [Di-E-GSSG] plots for un-acetylated and acetylated wt-PDI and PDI K-Q  $aa'$ . For each experiment the protein concentration was 20nM, and the initial rate was expressed as the amount of EGSH produced (nM/s). The assay was performed with 10 $\mu$ M of DTT in phosphate buffer (100mM phosphate pH 6.5, 0.1mM DTPA) and data was collected for 1 minute. The dashed lines represent the

application of the best-fit kinetic parameters, obtained from the data, to the Michaelis-Menten equation. The error bars represent standard deviation, n=3. .... 48

Figure 18. Michaelis-Menten kinetic parameters and catalytic efficiency ( $k_{cat}/K_M$ ) for wt-PDI and mutants. The kinetic parameters and catalytic efficiency were estimated from a fit of the initial rate data of EGSH production at pH 6.5 by wt-PDI and the Lys variants by using the Solver function in MS Excel. Results are expressed as the mean with standard deviation, n=3. Significant differences ( $p<0.05$ ) are indicated by \* ..... 50



## LIST OF ABBREVIATIONS/SYMBOLS

2xYT	Yeast Extract Tryptone
A	Alanine
ATase1	Acetyltransferase 1
ATase2	Acetyltransferase 2
BL21	E. coli B strain deficient in Lon protease
C	Cysteine
CBP	CREB-binding protein
CoA	Coenzyme A
Da	Dalton
Di-E-GSSG	Di-Eosin Glutathione disulfide
DMSO	Dimethylsulfoxide
DNase I	Deoxyribonuclease I
DTPA	Diethylene triamine pentaacetic acid
DTT	Dithiothreitol
E	Glutamic acid
EDTA	Ethylene Diamine Tetra Acetic Acid
EGSH	Eosin-Glutathione
ER	Endoplasmic reticulum
Gcn5	General control of amino-acid synthesis 5
Glu-C	Endoproteinase Glu-C
GNAT	GCN5-like N-acetyltransferase
GSNO	S-nitrosoglutathione
GSSG	Oxidized glutathione
GST	Glutathione S-transferase
H <sub>2</sub> O <sub>2</sub>	Hydrogen peroxide
HAT	Histone acetyltransferase
HCl	Hydrochloric Acid
IPTG	Isopropyl- $\beta$ -D-thiogalactopyranoside
K	Lysine
$k_{cat}$	Turnover rate
$K_M$	Michaelis constant
LB	Luria-Bertani
$m/z$	Mass-to-charge ratio
MALDI-TOF MS	Matrix assisted laser desorption ionization – time of flight mass spectrometry
Moz	Monocytic leukemic zinc-finger protein
MS/MS	Tandem-mass-spectrometry
MYST	Named after Moz, Ybf2, Sas2, and Tip60
NaOH	Sodium Hydroxide
NEB	New England Biolabs

NMR	Nuclear magnetic resonance
NO	Nitric Oxide
O <sub>2</sub>	Oxygen
p300	E1A binding protein p300
PAGE	Polyacrylamide gel electrophoresis
PCAF	p300-CBP-associated factor
PCR	Polymerase chain reaction
PDI	Protein disulfide isomerase
pH	Potential of hydrogen ion
p <i>K</i> <sub>a</sub>	Acid dissociation constant
PMSF	Phenylmethylsulphonyl fluoride
Q	Glutamine
RNase A	Ribonuclease A
Sas2	Something about silencing 2
SDS	Sodium Dodecyl Sulfate
SNO	<i>S</i> -nitrosylation
SOC	Super Optimal Broth that contains glucose
Tip60	Tat interactive protein-60
TRIS	Tris(hydroxymethyl)aminomethane
V <sub>Max</sub>	Maximum rate of reaction
wt	Wild type
Ybf2	Something about silencing 3

# Introduction

## 1.1 Protein folding and the importance of disulfide bonds

The unique functions carried out by proteins come in part due to their three-dimensional (3D) structure (Dill & MacCallum, 2012). Much scientific research has and still is being performed to understand how a one-dimensional chain of amino acids can quickly fold into the native protein structure (Dill & MacCallum, 2012). One of the hypotheses that try to explain the ability of an amino acid chain to quickly fold into the native state without stopping at any of the multiple stable conformations is the folding funnel hypothesis. This hypothesis states that the native structure of the protein has such a low free energy that it becomes unlikely that the protein will stay in a non-native stable conformation for long (Onuchic & Wolynes, 2004).

Predicting the mechanism of protein folding becomes more complex when considering the formation of a disulfide bonds within a protein (Narayan, 2012). A disulfide bond is a covalent bond between the thiol groups of two cysteines and plays an important role in protein folding and the stability of the native structure (Mamathambika & Bardwell, 2008). Disulfide bonds have also been shown to play functional roles at either the active site of proteins or at allosteric sites where they regulate enzyme activity (Mamathambika & Bardwell, 2008). Some of the major factors that affect disulfide bond formation are the concentration of thiolates, the accessibility of the thiols, the proximity of the thiols, and the reactivity of the thiols based on the microenvironment (Mamathambika & Bardwell, 2008). Incorrect disulfide bond formation can cause improper protein folding leading to protein aggregation followed by degradation (Mamathambika & Bardwell, 2008). This is the reason that proteins such as protein

disulfide isomerase are so important; they help with the formation, reduction, and/or isomerization of disulfide bonds (Mamathambika & Bardwell, 2008).

## **1.2 Protein disulfide isomerase (PDI)**

### *1.2.1 Overview*

The first reported observable activity of protein disulfide isomerase (PDI: EC 5.3.4.1) occurred in 1963 by Anfinsen's group. They observed the re-oxidation of RNase by rat liver microsomes fraction and from soluble nonprotein factors (Goldberger, Epstein, & Anfinsen, 1963). By 1964, Anfinsen's group was able to further purify the microsomes fraction to just a protein sample, where they correctly hypothesized that this protein may be able to facilitate the conversion of disulfide bonds on multiple proteins (Goldberger, Epstein, & Anfinsen, 1964). PDI was observed to reduce and isomerize disulfide bonds as well as oxidize thiols (Figure 1)(Holmgren, 1968). The active site sequence of rat PDI was later determined to be WCGHCK a similar sequence found in the thioredoxin family (Edman, Ellis, Blacher, Roth, & Rutter, 1985). It was later determined that PDI contains four thioredoxin-like domains and is now categorized as being a part of the thioredoxin superfamily (Alanen et al., 2003; Freedman et al., 1998). PDI is also the model protein for the PDI family, which contains 20 different isoforms (Kozlov, Maattanen, Thomas, & Gehring, 2010).

In 1994, it was discovered that PDI possess chaperone activity in addition to the aforementioned thiol redox activity (Cai, Wang, & Tsou, 1994). It was later determined that this chaperone activity worked independently of the redox status of active site

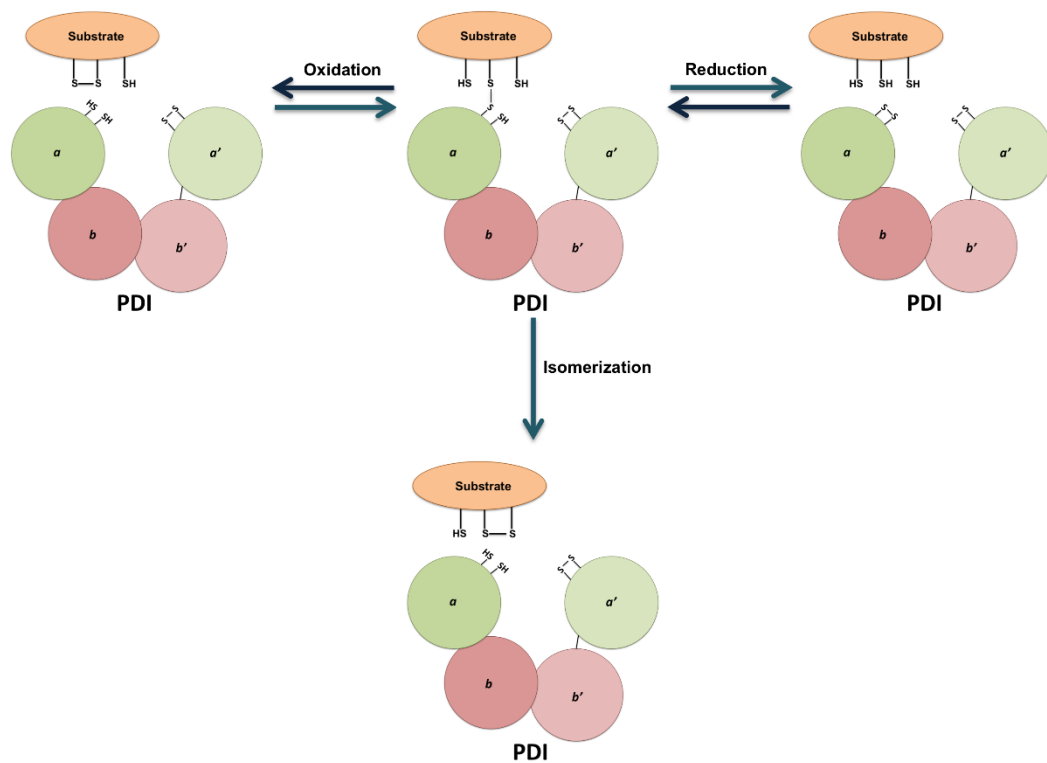


**Figure 1.** The 3 main redox reaction catalyzed by PDI: oxidation of thiols, reduction of disulfide, and isomerization of disulfide.

thiols (McLaughlin & Bulleid, 1998). The three catalytic activities of PDI, thiol redox, disulfide exchange, and chaperone are central to endoplasmic reticulum (ER) function, where PDI is highly expressed (Maattanen, Gehring, Bergeron, & Thomas, 2010). Although PDI has a C-terminal KDEL ER retention sequence, significant amounts of this protein were shown to escape the ER and were detected in the nucleus, cytosol, cell surface, and extracellularly (Edman et al., 1985; Koch, 1987; Yoshimori et al., 1990). It is important to state that PDI is expressed in almost all mammalian tissues, playing important role in redox and chaperone activity (Marcus, Shaffer, Farrar, & Green, 1996; Noiva, 1999).

### *1.2.2 Structural importance of PDI and the interplay with catalytic activity*

All members of the PDI family contain at least one thioredoxin-like domain structure characterized as a  $\beta\alpha\beta\alpha\beta\alpha\beta\alpha$  fold (Kemink, Darby, Dijkstra, Nilges, & Creighton, 1997). PDI is comprised of 5 domains *abb'a'c* where *abb'a'* are thioredoxin-like domains and *c* is an acidic domain (Figure 2)(Freedman et al., 1998; Koivunen et al., 1999). In the *c* domain there is an ER retention sequence KDEL at the C-terminal (Edman et al., 1985). The *a* and *a'* domains contain the thiol redox catalytic motif CXXC, whereas the *b* and *b'* domains do not contain this motif (Freedman et al., 1998). There is a small chain of amino acids between the *b'* and *a'* domains known as the x-linker, which is believed to provide some flexibility to the protein (C. Wang et al., 2013). The N-terminal cysteine in the catalytic motif (CXXC) is observed to have a pKa of 4.8 whereas the C-terminal cysteine (CXXC) pKa is reported to be 10 (Karala, Lappi, & Ruddock, 2010; Nelson & Creighton, 1994). The low pKa of the N-terminal cysteine will

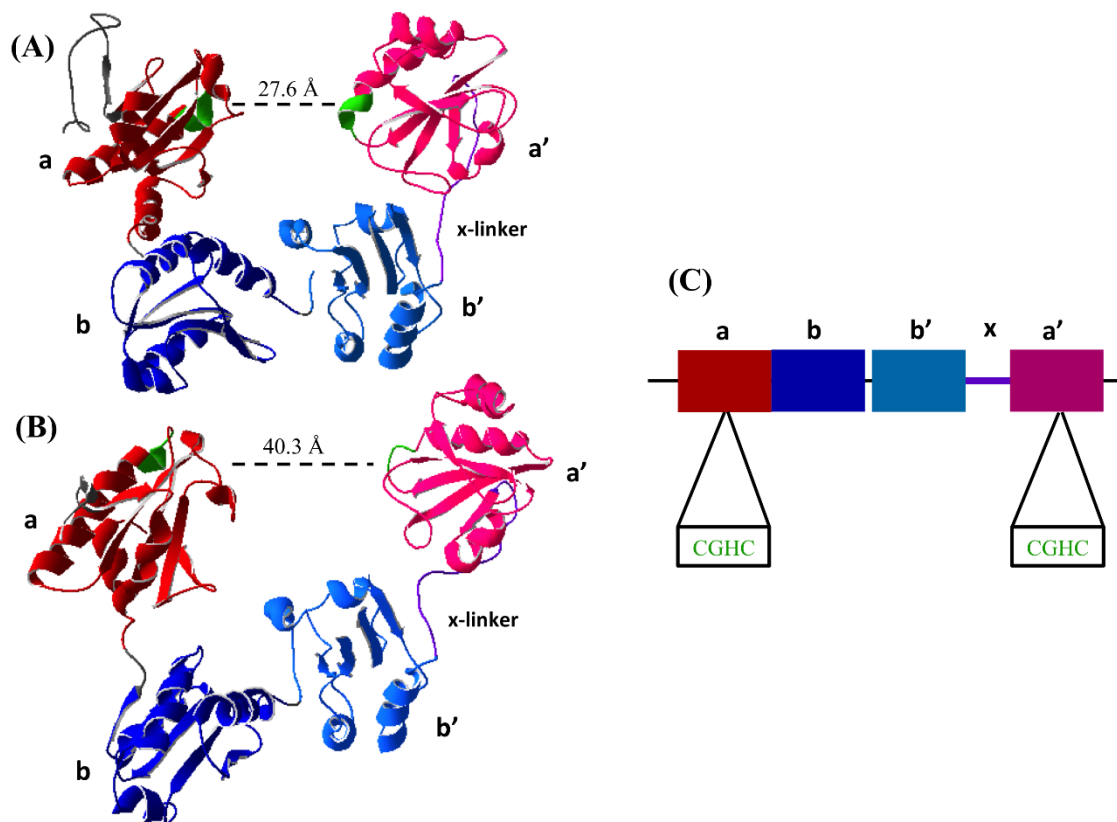


**Figure 2.** Crystal Structure of Reduced and Oxidized PDI. (A) Reduced crystal structure of human PDI (PDB ID: 4EKZ). (B) Oxidized crystal structure of human PDI (PDB ID: 4EL1). (C) Schematic of PDI domains present in the crystal structure, as well as the two active site CXXC motifs. (Crystal structures created using Swiss PDBViewer). Image taken from Khan, H. A., & Mutus, B. (2014). *Frontiers in chemistry*, 2.

result in a higher percentage of the more reactive thiolate to form. This supports the reasoning that the N-terminal cysteine reacts with the substrate first to form a mixed disulfides (Walker & Gilbert, 1997). The high pKa of the C-terminal cysteine keeps the majority as a thiol allowing for this cysteine to help with the release of the substrate (Walker & Gilbert, 1997). This process is suggested to greatly help PDI from being trapped in a mixed disulfide bond with a substrate (Walker & Gilbert, 1997). It is hypothesized that PDI performs a “scanning and escape” mechanism, where after forming a mixed disulfide PDI will scan for other thiols that are thermodynamically stable to react with the substrate (Walker & Gilbert, 1997). If no thiol is available the C-terminal will help PDI “escape” from being trapped in a mixed disulfide with the substrate (Walker & Gilbert, 1997). Interestingly, both the *a* and *a'* domains contain a lysine on the C-terminal end of the catalytic motif (CXXCK)(Edman et al., 1985).

The redox-inactive *b* and *b'* domain has been identified to exhibit chaperone activity (Denisov et al., 2009). Through NMR, the structure and amino acid residues of the *b'* domain were observed to interact with unfolded RNase A, an oft used enzyme to assay the chaperone activity of PDI. The *b'* domain contains a large multivalent hydrophobic surface allowing for a structurally promiscuous binding site (Denisov et al., 2009). In addition, computational analysis indicates that the *bb'* domains contain 4 cavities allowing for the possible binding of a variety of ligands (Fu, Wang, & Zhu, 2011). Recently human PDI was found to dimerize *in vivo* through the binding of *bb'* (Ali Khan & Mutus, 2014; Bastos-Aristizabal, Kozlov, & Gehring, 2014).

Recently was observed that the chaperone activity of PDI is regulated by its redox status. The crystal structure of the four thioredoxin-like domains of PDI in both the



reduced and oxidized forms were obtained (C. Wang et al., 2012). The oxidized form of PDI, the active site of *a* and *a'* are 40.3 Å apart and the thioredoxin domains *abb'a'* were all in the same plane (Figure 2B)(C. Wang et al., 2012). Whereas in the reduced state of PDI the active sites are 27.6 Å (Figure 2A), and only *abb'* are in the same plane where *a'* is twisted 45°, illustrating that the oxidized state has a more open conformation allowing for the entry of chaperone substrates and the reduced state has a closed conformation inhibiting their entry (C. Wang et al., 2013). This further illustrates long range conformational changes induced by redox status of the active sites and further suggests redox regulation of chaperone activity (Ali Khan & Mutus, 2014).

### *1.2.3 PDI localization/protein interactions/physiological role*

As stated above, PDI contains an ER retention sequence at the C-terminal (Edman et al., 1985). PDI is highly expressed in the ER, where its concentration is estimated to be in the millimolar range (L. Wang, Wang, & Wang, 2015). This high concentration allows PDI to function as a catalyst for oxidative protein folding through its redox activity. As well as function as a chaperone at stoichiometric concentrations on nascent polypeptides as well as on improper folded proteins (L. Wang et al., 2015). As PDI performs its redox activity within the ER, it is suggested that an oxidized *a* domain catalyzes the oxidation of the reduced substrates and in the process becomes reduced (Walker & Gilbert, 1997). The *a* domain is then subsequently oxidized by the *a'* domain back to a disulfide through intramolecular reactions (Araki et al., 2013). The re-oxidation of the *a'* domain is catalyzed by the protein endoplasmic reticulum oxidoreductin-1 (Ero1) in the process reducing O<sub>2</sub> to produce H<sub>2</sub>O<sub>2</sub> (Figure 3) (Ali Khan & Mutus, 2014; Araki & Nagata, 2011). It is also worth noting that glutathione and glutathione disulfide

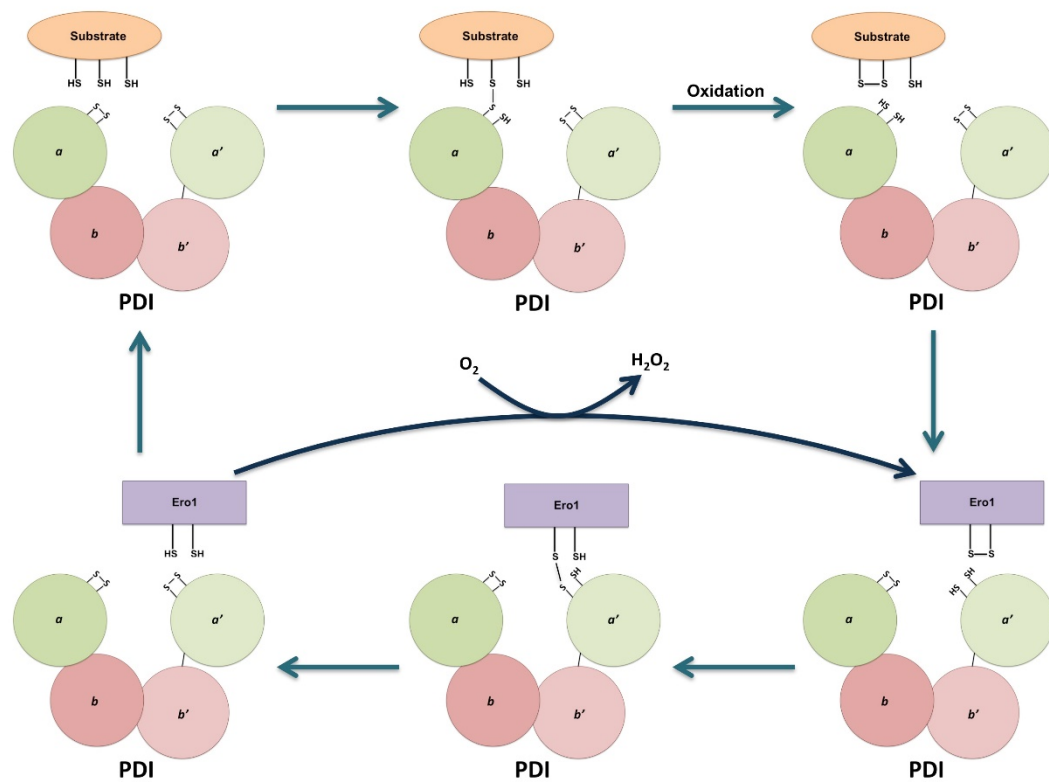


**Figure 3.** The hypothesized regeneration of PDI by Ero1. The *a* domain of PDI oxidizes the substrate. The now reduced *a* domain is re-oxidized by the *a'* domain. The now reduced *a'* domain is re-oxidized by Ero1. The thiols of Ero1 are oxidized by  $O_2$ .

(GSH/GSSG) can also oxidize and reduce the  $\alpha$  and  $\alpha'$  domain (Ali Khan & Mutus, 2014). As a chaperone PDI has been observed to refold proteins such as glyceraldehyde-3-phosphate dehydrogenase, rhodanese, citrate synthase, and alcohol dehydrogenase (Wilkinson & Gilbert, 2004). It has also been observed that PDI can act as an anti-chaperone, where it can cause substrate protein-aggregation resulting in precipitation (Wilkinson & Gilbert, 2004).

As previously stated, PDI is shown to be secreted to the cell surface of multiple cell types (Turano, Coppari, Altieri, & Ferraro, 2002). Many studies have shown that cell surface PDI plays a role in platelet activation (Ali Khan & Mutus, 2014; Turano et al., 2002). Thiols on the surface of platelets play a critical role in integrin-mediated platelet adhesion, where PDI is required for the reduction and reshuffling of disulfide bonds (Turano et al., 2002). Overall, PDI has been observed to play multiple roles in blood clot formation (Ali Khan & Mutus, 2014; Cho, 2013; Flaumenhaft, 2013). Cell surface PDI has also shown to play a role in nitric oxide signalling (Ali Khan & Mutus, 2014; Ramachandran, Root, Jiang, Hogg, & Mutus, 2001). Cell surface PDI was observed to release NO from S-nitrosylated glutathione (GSNO), one of the main nitric oxide carriers in tissues (Root, Sliskovic, & Mutus, 2004). PDI would denitrosylate GSNO when NO levels were low, however during high levels of NO, PDI would act as a carrier either through the formation of SNO-PDI (Ali Khan & Mutus, 2014; Sliskovic, Raturi, & Mutus, 2005).

Within liver cells, PDI is observed to be present in high quantities in the cytosol (Turano et al., 2002). PDI is proposed work as an insulin degrading enzyme, where it degrades insulin through the reduction of its disulfide bonds (Turano et al., 2002). In the

nucleus, PDI is observed to affect the activity of transcription factor E2A. As well PDI has been observed to interact with estrogen receptors to help with DNA binding (Turano et al., 2002).

#### *1.2.4 Catalytic activity assays for PDI*

Since PDI has multiple functions, there are many diverse assays to detect these activities. Each assay will only detect one of the four functions of PDI. Majority of the assays for the PDI isomerase activity, deal with gain-of-function of an inactive protein that contains incorrectly formed disulfide bonds (Watanabe, Laurindo, & Fernandes, 2014). The two main proteins used for isomerase activity assays are scrambled RNase and riboflavin-binding protein (Watanabe et al., 2014). With scrambled RNase, the addition of PDI will result in refolding to the native structure of RNase (Watanabe et al., 2014). As RNase refolds, it will start to hydrolyze cyclic cytidine monophosphate, which can be detected by absorbance (El Hindy et al., 2013; Lyles & Gilbert, 1991; Watanabe et al., 2014).

Oxidation assays can be performed similar to isomerase assays where gain-of-function is observed. Another possible assay to detect oxidative folding is to trap intermediates of oxidative folding by PDI using thiol alkylating agents, followed by mass spectrometry (Watanabe et al., 2014). For chaperone activity, again gain-of-function assays can be used, ensuring that proteins-substrates do not have disulfides in native conformation i.e. glyceraldehyde-3-phosphate dehydrogenase (Cai et al., 1994; Watanabe et al., 2014).

The most common reduction assay is the reduction of insulin by PDI resulting in the precipitation of insulin (Watanabe et al., 2014). The turbidity of the solution can be

monitored to determine reductase activity of PDI (Holmgren, 1979; Watanabe et al., 2014). However, for this assay the lag time for precipitation to start and the rate of precipitation must be taken into account (Watanabe et al., 2014). Another reductase assay produced by our research group, uses GSSG where eosin-isothiocyanate, a fluorescent molecule, is covalently bonded to the two amine groups, it is known as dieosin glutathione disulfide (Di-E-GSSG) (Figure 4)(Raturi & Mutus, 2007). Di-E-GSSG is not fluorescent due to the close proximity of the eosin moieties resulting in self-quenching. When PDI is present the disulfide bond is reduced resulting in two eosin glutathione (EGSH) molecules, which are fluorescent (Raturi & Mutus, 2007). The reduction of Di-E-GSSG to EGSH results in a ~70 fold increase in fluorescence. This assay requires low amounts of dithiothreitol (DTT), a thiol reducing agent, to re-reduce the PDI active site thiols. DTT at the concentrations employed (~50  $\mu$ M) agent does not reduce Di-E-GSSG (Raturi & Mutus, 2007). This assay only requires nanomolar amounts of PDI, which makes this the most sensitive assay for PDI reductase activity to date.

### **1.3 Acetyltransferases**

The transfer of an acetyl moiety from acetyl-CoA to the  $\epsilon$ -amino group of a lysine was first observed in 1960 on histones (Marmorstein, 2001). This reversible post-translational modification results in the neutralization of the lysine as well as impairs hydrogen bonding and creates a bulkier side chain (Figure 5) (Dormeyer, Ott, & Schnolzer, 2005; Lee & Workman, 2007; Patel, Pathak, & Mujtaba, 2011). The enzymes that catalyze this reaction are termed acetyltransferase. At first this modification was thought to occur only on histones, however recently, non-histone proteins were observed to be acetylated (Pehar & Puglielli, 2013). It was believed that protein acetylation could

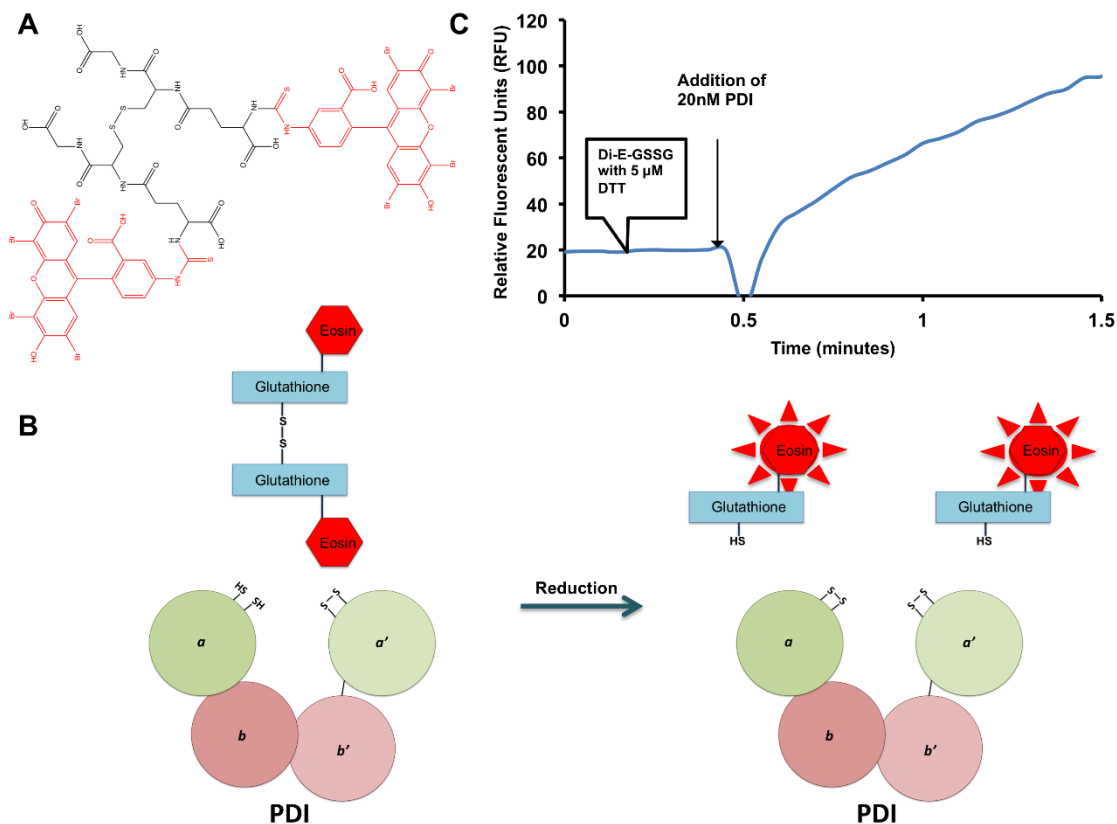


**Figure 4.** Fluorogenic Di-E-GSSG reductase assay. A) Structure of Di-E-GSSG. B) Reduction mechanism of Di-E-GSSG by PDI to produce the fluorescent EGSH. C) Fluorescent graph of reductase assay, where DTT demonstrates little increase in fluorescence. With the addition of PDI, fluorescence increases.

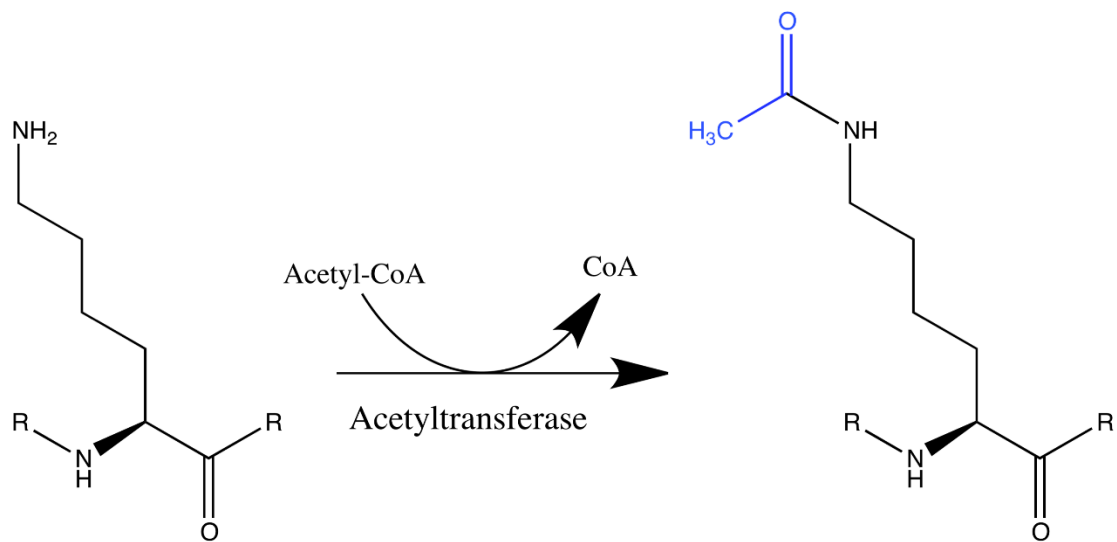


**Figure 5.** Lysine acetylation by acetyltransferase and acetyl-CoA.

only occur in the nucleus and cytosol since that was the only area where it was observed. However recently protein acetylation was observed in the mitochondria, and more recently in the ER (Pehar & Puglielli, 2013).

There are three main families of acetyltransferases; MYST, p300/CBP, and Gcn5-related N-acetyltransferase (GNAT)(Spange, Wagner, Heinzl, & Kramer, 2009). The MYST protein family is named after four members of the family; MOZ, Ybf2, Sas2, and Tip60 (Marmorstein, 2001). This protein family has sequence similarities at the acetyl-CoA binding motif with the GNAT family (Aka, Kim, & Yang, 2011). The p300/CBP do not have this acetyl-CoA binding motif and do not share sequence similarities with GNAT family or MYST family (Aka et al., 2011). The protein p300 appears to have a very broad substrate acetyltransferase. The GNAT family is the largest acetyltransferase family, containing proteins such as p300/CBP-associated factor (PCAF) and general control nonrepressed 5 (Gcn5)(Aka et al., 2011). This family all possess four conserved sequence motifs known as C, D, A, and B (Pehar & Puglielli, 2013).

The only two acetyltransferases observed in the ER belong to the GNAT family of acetyltransferases. These two proteins known as ATase1 (also known as N-acetyltransferase 8B) and ATase2 (also known as N-acetyltransferase 8) are also members of the camello family (Pehar & Puglielli, 2013). These proteins are differentially expressed in a variety of cells. Interestingly *in vitro* experiments show that ATase 1 undergoes auto-acetylation, whereas ATase2 does not auto-acetylate (Pehar & Puglielli, 2013). It is important to remember that acetylation requires acetyl-CoA, which therefore means that acetyl-CoA must be transported into the ER. Experiments have revealed that there is a carrier-mediated transporter of acetyl-CoA on the ER membrane, where CoA



moiety is the detection signal (Pehar & Puglielli, 2013). There have only been two observed acetyltransferases in the ER, however it is likely that there are other ER-based acetyltransferases (Pehar & Puglielli, 2013). Recently, a proteomic study was conducted to discover all ER acetylated proteins (Pehar, Lehnus, Karst, & Puglielli, 2012). Over 100 proteins were identified to be ER acetylated proteins, by confirmation through mass spectrometry (Pehar et al., 2012). PDI was one of these proteins signifying that acetylation may regulate PDI activity. It was observed that lysine at the  $\alpha'$  domain (K401) was observed to be acetylated. This sparked our interest, as a possible post-translational modification to regulate PDI activity.

#### **1.4 Research objectives**

Very little research has been conducted on the regulation of PDI. The goal of this project is to determine whether reductase activity is affected by a PDI-acetylation and to identify the regulatory lysine residues in the enzyme. PDI acetylation will be investigated by an acetyltransferase (PCAF) as well as by chemical acetylation by acetic anhydride. The candidate lysine residues are those flanking the active site motif of PDI. Mutant variants of these two lysines will be produced to see their effects on the reductase activity of PDI. Mass spectrometry will be used in conjunction with activity assays to identify the sites of acetylation.

## Materials

### 2.1 Chemicals

- Tryptone, and yeast extract were purchased from Bio Basic Inc.
- Sodium phosphate dibasic, sodium phosphate monobasic, glycerol, sodium chloride, and sodium carbonate were purchased from ACP Chemicals Inc.
- Dithiothreitol was purchased from MP Biomedical.
- Bis-acrylamide solution, and Bio-Rad Protein Assay were purchased from Bio-Rad.
- Tris hydrochloride, dimethyl sulfoxide (DMSO), sodium dodecyl sulphate, Tris base, potassium phosphate dibasic, potassium phosphate monobasic, kanamycin, bromophenol blue, ammonium persulfate, ammonium bicarbonate, and agarose were purchased from Fisher Scientific.
- Acetic anhydride, sodium butyrate, imidazole, boric acid, sodium acetate, sodium azide, Triton X100, bovine serum albumin, lysozyme, ethylenediaminetetraacetic acid (EDTA), isopropyl  $\beta$ -D-1-thiogalactopyranoside (IPTG), Coomassie Brilliant Blue R, deoxyribonuclease I from bovine pancreas (DNase I), trifluoroacetic acid,  $\alpha$ - cyano-4-hydroxycinnamic acid, phenylmethanesulfonyl fluoride (PMSF), diethylenetriaminepentaacetic acid (DTPA), His Select™ Nickel Affinity gel, Glutathione–Agarose, chloramphenicol, reduced glutathione, glutathione disulfide, 5,5'-dithiobis-(2-nitrobenzoic acid), Sephadex G-25, bicinchoninic acid, copper(II) sulfate pentahydrate, guanidine hydrochloride, nickel(II) sulphate, TEMED, and Phenol:Chloroform:Isoamyl alcohol25:24:1 were purchased from Sigma-Aldrich.

- Zeba™ spin desalting columns was purchased from Thermo Scientific.
- Plasmid Mini Kit was purchased from Qiagen.
- Trypsin and Glu-C mass spec grade were purchased from Promega.
- Bacteriological agar was purchased from Quelab.
- PageRuler Plus Prestained Protein Ladder, GeneRuler 1 kb DNA Ladder, and Eosin-5-Isothiocyanate were purchased from Life Technologies.
- Magnesium chloride was purchased from BDH VWR analytical.
- Q5® Site-Directed Mutagenesis Kit, NEB 5-alpha competent cells, PvuII, AvaI, AvaII, NaeI, NotI, SmaI SacI, XmnI, and EcoRI were purchased from New England BioLabs.
- BL21 DE3 pLys competent cells was purchased from EMD Millipore.

## 2.2 Plasmids and primers

- The pEt22b plasmid containing recombinant human PDI was created by Dana Seslija.
- The pGEX-2T plasmids containing GST-PCAF-HAT was kindly donated by Dr David LeBrun from Queens University.
- All primers were made by Intergrated DNA Technology:
  - Reverse PDI *a* domain primer:  
5'AGGGGCCAGAGCCGCGCAGTGGCCACACCAAGG3'
  - PDI Lys-Ala *a* domain primer:  
5'AGGGGCCAGAGCCGCGCAGTGGCCACACCAAGG3'
  - PDI Lys-Gln *a* domain primer:  
5'AGGGGCCAGAGCCTGGCAGTGGCCACACCAAGG3'

- PDI Lys-Glu *a* domain primer:  
5'AGGGGCCAGAGCCTCGCAGTGGC3'
- Reverse PDI *a*' domain primer:  
5'CCATGGGGCATAGAATTCCACAAAGAC3'
- PDI Lys-Ala *a*' domain primer:  
5'TGTGGTCACTGCGCACAGTTGGCTCCC3'
- PDI Lys-Gln *a*' domain primer:  
5'TGTGGTCACTGCCAACAGTTGGCTCCC3'
- PDI Lys-Glu *a*' domain primer:  
5'TGTGGTCACTGCGAACAGTTGGCTC3'
- Reverse PDI cysteine 295 primer:  
5'TCAGGCCAAAGAACTCTAGGATGCG3'
- Forward PDI cysteine 295 to serine primer:  
5'AGAAGGAAGAGTCCCCGGCCGTGCG3'
- Reverse PDI cysteine 326 primer:  
5'TCCTCTCTGCCGTGAGCTCCTCCGATTC3'
- Forward PDI cysteine 326 to serine primer:  
5'TCACAGAGTTCTCCCACCGCTTCCTGGA3'

### 2.3 Equipment

- Bio-Rad; PowerPac™ High current power supply, electrophoresis chamber, Mini-Sub® cell GT cell, T100™ Thermal Cycler, and Fraction Collector Model 2110.
- Fisher Scientific; Model 100 Sonic Dismembrator.
- Perkin Elmer; Wallac 1420 Victor 3 Fluorescent Plate Reader.

- PGC Scientifics; Type 37900 Culture Incubator.
- Thermo Electron Corp; Orion Model 420A pH Meter, and Centrifuge Jouan BR4i.
- Alpha Innotech Corporation; AlphaImager<sup>®</sup> serial number 200018.
- Agilent Technologies; Agilent 8543 UV-VIS Spectrophotometer, and Varian Cary Eclipse Fluorescence Spectrophotometer.
- New Brunswick Scientific; C25 Incubator Shaker.
- EMD Millipore; 30kDa Amicon Ultra-15 Centrifugal Filter Units.
- Molecular Devices; SpectraMax<sup>®</sup> Plus 384 Absorbance plate reader.
- Labconco; Freeze dry system/Freezone 4.5.
- Beckman Coulter; Beckman J2-HS centrifuge.
- Applied Biosystems; Voyager-DE Pro Workstation mass spectrometry.
- Hettich Zentrifuge; EBA-12 centrifuge.
- Mettler Toledo; AJ100 analytical balance.
- Ohaus; Scout Pro balance.

## Methods

### 3.1 Plasmid bacterial transformation

The protocol used was obtained from Q5® Site-Directed Mutagenesis Kit Protocol from New England BioLabs with minor changes. BL21, NEB 5-alpha, or Gold competent cells were thawed on ice. Approximately 1-50ng of plasmid was then added to 20µL of competent cells and was mixed by flicking. Competent cells were returned onto ice for 30 minutes. Competent cells were then heat shocked by incubating cells in 42°C water bath for 30 seconds. Cells were returned to ice and incubated for 2 minutes. The SOC outgrowth medium was added to cells and then incubated in the C25 Incubator Shaker at 37°C for 60 minutes at 220 rpm. After incubation 100µL of cells were plated on either LB agar plates (Gold and NEB 5-alpha) or 2xYT agar plates (BL21) and incubated overnight at 37°C. After incubation colonies were picked and added to LB or 2xYT media. The culture was then incubated overnight where either mini-prep or protein purification was performed.

### 3.2 Bacterial mini prep

The Qiagen Mini Prep protocol was used with some modifications to the protocol. After plasmid transformation, 1.5 mL of culture was centrifuged for 1 minute at 12000 x g. The medium was then aspirated in order to obtain a dry pellet. The pellet was re-suspended with 100µL of Buffer P1(50mM glucose, 25 mM Tris HCl, 10mM EDTA) from the Qiagen Mini Kit. Qiagen Mini Kit Buffer P2 (0.2N NaOH, 1% SDS), 250µL was added and was mixed by inversion. This was followed by 150µL of Buffer P3(3M sodium acetate pH 5.2) from the Qiagen Mini Kit was again mixed by inversion. The sample was then centrifuged at 12000 x g for 30 minutes at 4°C. Phenol:chloroform,

400µL was added to the supernatant. The mixture was then vortexed and centrifuged at 12000 x g for 1 minute at room temperature. The top aqueous phase was collected and 800µL of ice cold 95% ethanol was added. The sample was then vortexed and centrifuged at 12000 x g for 10 minutes at 4°C. The supernatant was decanted and 400µL of ice cold 70% ethanol was added to the pellet, which was then centrifuged at 12000 x g for 1 minute at room temperature. The supernatant was decanted and the pellet was air dried in an inverted position for 10 minutes, re-suspended in 30µL of TE buffer (10mM Tris, 1mM EDTA pH 8) containing 20µg/mL of RNase A and incubated at 37°C for 15 minutes. At this point the plasmid was either used for further experiments or frozen at -80°C.

### **3.3 Site-directed mutagenesis**

The Q5® Site-Directed Mutagenesis Kit protocol was used with minor changes. The primers were designed to be end-to-end where the forward primer contained the mutation and the reverse primer resulted in the gain or loss of a restriction enzyme digest site. The PCR mix contained 6.25µL of the Q5 Hot Start High Fidelity 2x Master mix, 0.625µL of the forward and reverse primer, 0.5µL of the template plasmid, and 4.5µL of nuclease-free water. Using the T100™ Thermal Cycler the cycling conditions were set according to Q5® Site-Directed Mutagenesis Kit. The initial denaturation step occurs at 98°C for 30 seconds. The amplification cycle was repeated for 25 cycles of first a 10 second denaturing step at 98°C. This was followed by 30 seconds of annealing at a temperature between 50°C and 72°C depending on the primers used. The annealing temperatures were calculated by the addition of 3°C to the melting temperature of the primer. The elongation step occurred next for 30 seconds at 72°C. After the 25 cycles, a

final step of elongation occurred for 2 minutes at 72°C. After PCR, 1µL of the PCR product was treated with 1µL of a kinase, ligase, DpnI mixture, 5µL of the reaction buffer, and 3µL of nuclease-free water. This mixture was mixed by pipetting and kept at room temperature for 5 minutes, where bacterial transformation followed.

### **3.4 Protein purification**

#### *3.4.1 His-Tagged PDI protein purification*

The protein purification of PDI followed the same protocol of Raturi et al. with some modifications (Raturi & Mutus, 2007). The expression of human PDI in pEt22b plasmid was transformed in *E. coli* BL21. Cells were grown in 2xYT (tryptone, yeast extract, and sodium chloride) with antibiotics (10µg/mL kanamycin A, 25µg/mL chloramphenicol) at 37°C until the OD<sub>600</sub> reading was between 0.4 – 0.6. Expression of plasmid was induced with 1mM isopropyl β-D-1-thiogalactopyranoside and the cells were incubated for 4 hours. Centrifugation of the cells were centrifuged at 6000 rpm for 30 minutes at 4°C and re-suspended in lysis buffer (1mM sodium chloride, 50mM Tris hydrochloride (pH 8), 100µg/mL lysozyme, 50µg/mL DNase I, 2mM PMSF, and 1% Triton X100) for 30 minutes on ice. The mixture was sonicated with a Fisher Scientific Model 100 Sonic Dismembrator at a power level of 4, for 8 pulses, 20 seconds in duration. The lysate was centrifuged at 10000 rpm at 4°C for 30 minutes. The supernatant was applied to the His Select<sup>®</sup> Nickel Affinity column that was equilibrated with wash buffer (10mM imidazole, 50mM sodium phosphate, 150mM sodium chloride pH 8). The column was washed with 3 column volumes of wash buffer. Elution buffer (250mM imidazole, 50mM sodium phosphate, 150mM sodium chloride pH 8) was then used to elute the protein of interest. The protein sample was reduced using 1M of DTT. Buffer



exchange was then performed on the protein fractions with a 30kDa Amicon Ultra-15 Centrifugal Filter Unit exchanging with 100mM phosphate buffer (100 $\mu$ M DTPA pH 7.4). Protein concentration was determined using the BCA assay where bovine serum albumin was used as the standard. Protein purity was determined by a 10% SDS-PAGE and stained with Coomassie Brilliant Blue.

#### 3.4.2 *GST-Tagged protein purification*

The expressions of GST-tagged proteins in the pGEX-2T plasmids were transformed into *E. coli* BL21. Cells were grown in 2xYT (tryptone, yeast extract, and sodium chloride) with antibiotics (10 $\mu$ g/mL ampicillin, and 25 $\mu$ g/mL chloramphenicol) at 37°C until the OD<sub>600</sub> reading was between 0.4 – 0.6. Expression of plasmid was induced with 1mM isopropyl  $\beta$ -D-1-thiogalactopyranoside and the cells were incubated for 4 hours. The lysate was centrifuged at 10000 rpm for 30 min at 4°C. The cells were then re-suspended in lysis buffer (1mM sodium chloride, 50mM Tris hydrochloride (pH 8), 100 $\mu$ g/mL lysozyme, 50 $\mu$ g/mL DNase I, 2mM PMSF, and 1% Triton X100) for 30 minutes on ice. The cells were then sonicated with the tip of a Fisher Scientific Model 100 Sonic Dismembrator at a level of 4, for 8 pulses, 20 seconds in duration. The lysate was centrifuged at 10000 rpm for 30 min at 4°C. The supernatant was applied to a glutathione-agarose column, followed by 4 column washes of the resin with PBS-T (10mM phosphate buffer, 150mM sodium chloride, 1% Triton X100, pH 7.4). The protein of interest was then eluted with elution buffer (10mM reduced glutathione, 50mM Tris-HCl, pH 9.5). Buffer exchange was then performed with a 30kDa Amicon Ultra-15 Centrifugal Filter Units with 100mM phosphate buffer (100 $\mu$ M DTPA pH 7.4). Protein concentration was determined using the BCA assay where bovine serum albumin was

used as the standard. Protein purity was determined by 10% SDS-PAGE and stained with Coomassie Brilliant Blue.

### **3.5 Di-Eosin-Glutathione Disulfide (Di-E-GSSG) synthesis**

Di-E-GSSG was synthesized as per Raturi et al. with some minor modifications (Raturi & Mutus, 2007). In a 50mL conical tube, 20mg of glutathione disulfide was dissolved with 1mL of 100mM ammonium bicarbonate buffer (2mM EDTA, pH 9). A 2.5 molar excess of eosin-5-isothiocyanate was weighed out in the dark and dissolved in 2mL of DMSO. The solution of eosin-5-isothiocyanate was slowly added to the 50mL conical tube containing glutathione disulfide while it was being vortexed at a low setting. The solution was brought to a total volume of 10mL with 100mM ammonium bicarbonate buffer. The reaction was incubated at 4°C overnight on a nutating mixer. The reaction was then quickly frozen by rotating the conical tube in a dewar of liquid nitrogen. The sample was then lyophilized overnight, where the remaining solid was dissolved with 1mL of milli-Q water. The 1mL of lyophilized sample was then applied to a sephadex G-25 column containing 50mL of resin, which was equilibrated with 10mM phosphate buffer (2mM EDTA, pH 7.4). Using a fraction collector, 180 fractions were collected each containing 1mL of eluate. Fractions are then tested to observe amount of fluorescent fold increase, by obtaining 20 $\mu$ L of the fraction and adding 1M of DTT in a 96-well plate. The increase in fluorescence was monitored at a wavelength of 545nm with an excitation wavelength of 525nm. Fractions that showed a >30 fold or increase in fluorescence were pooled. The concentration of the Di-E-GSSG was obtained from the extinction coefficient of eosin (176000M<sup>-1</sup>·cm<sup>-1</sup> at 525nm. Di-E-GSSG solution was then divided into small aliquots and stored at -80°C.

### **3.6 Quantification of Eosin Reduced Glutathione (EGSH)**

Known concentration of Di-E-GSSG were reduced with 5M DTT and incubated for 30 minutes at room temperature to produce 2 EGSH. The fluorescence of the samples was measured at 545nm (ex 525nm) and a standard curve of fluorescence vs. [EGSH] was generated. This standard curve was used to quantify the concentration of EGSH that was produced from the PDI-mediated reduction of Di-E-GSSG.

### **3.7 Determination of PDI concentration through burst kinetics**

The concentration of PDI and the lysine variants were determined through burst kinetics. The experiment consisted of 10 $\mu$ L of enzyme that was reacted with 800nM of Di-E-GSSG in 100mM phosphate buffer (pH 7.4, 100 $\mu$ M DTPA) for 10 minutes. The reaction was excited at 525nm and the fluorescence was monitored at 545nm. The linear regression was obtained after the burst phase, where the y-intercept corresponds to the amount of enzyme. Using the EGSH standard curve the concentration of enzyme was determined.

### **3.8 PDI kinetic assay**

The protocol for PDI reductase activity assay was obtained from Raturi et al. with some minor modifications (Raturi & Mutus, 2007). The buffer used for all kinetic activity assays was 100mM phosphate buffer containing 100 $\mu$ M DTPA at pH 7.4. The buffer was filtered using a 0.2 $\mu$ m filter, degassed and purged with argon gas. Using the Varian Cary Eclipse Fluorescence Spectrophotometer, 20 $\mu$ M of PDI or mutant PDI was added to varying concentration of Di-E-GSSG (5nM-6000nM) in the presence of 10 $\mu$ M DTT. The sample was excited with 525nm light and the fluorescence monitored at 545nm. For the

pH titrations of PDI, the concentration of Di-E-GSSG was kept at 400nM and the pH varied from 5.5 to 7.5. All kinetic assays are performed in triplicates.

### **3.9 PDI acetylation**

#### *3.9.1 PDI Acetylation by acetyltransferase*

The protocol for *in vitro* acetylation was taken from Ogryzko et al. with some changes(Ogryzko, Schiltz, Russanova, Howard, & Nakatani, 1996). The amount of the acetyltransferases, (PCAF) used for the acetylation of PDI was in a 2:1 molar ratio. Where 300pmol of PDI and 600pmol of acetyltransferase were dissolved in 500µL of acetylation buffer. The acetylation buffer consisted of 50mM Tris hydrochloride pH 8, 50mM sodium chloride, 2.5mM magnesium chloride, 10mM sodium butyrate, 10% glycerol, 0.5mM PMSF, 0.5mM DTT, and 6nM of acetyl-CoA, where DTT and acetyl-CoA are added fresh to the buffer before use. The reaction proceeded for 2 hours at 30°C on a nutating or rotating mixer. PDI was then isolated by using the His Select<sup>®</sup> Nickel Affinity trial purification protocol found on the product information sheet. All eluate was kept to determine any loss of PDI by running the samples on a 10% SDS-PAGE. The isolated PDI was then buffer exchanged using Zeba<sup>™</sup> spin desalting columns. The modified PDI sample was then frozen and kept for mass spectrometry.

#### *3.9.2 PDI acetylation by acetic anhydride*

Acetic anhydride was used for the chemical acetylation of lysines on PDI. 4µmol of PDI was reacted with either 8µmol or 40µmol of acetic anhydride. The reaction was incubated at 4°C for 2 hours on a rotating mixer. After incubation the modified PDI was

then buffered exchanged using using Zeba™ spin desalting columns. The modified PDI sample was then frozen and kept for mass spectrometry or kinetic assays.

### 3.10 Mass spectrometry analysis of PDI

PDI samples were digested using Glu-C for analysis on MALDI-TOF (Voyager-DE Pro Workstation mass spectrometry) and LC-MS. A 10:1 protein to protease by mass ratio was maintained for all digests. PDI was digested overnight at room temperature. The samples were then cleaned following manufacture's protocol, and spotted with a 1:1 ratio of 10mg/mL of matrix solution ( $\alpha$ -cyano-4-hydroxycinnamic acid in 60% acetonitrile, 0.1% trifluoroacetic acid). The digests were analyzed by matrix assisted laser desorption ionization-time of flight mass spectrometry (MALDI-TOF MS). Tandem mass spectrometry (MS/MS) was performed on active site parent ions and compared to sequence fragments predicted by Protein Prospector Software (<http://prospector.ucsf.edu/>).

### 3.11 Computational analysis

In collaboration with Dr. Gaulds Group, computational analysis was performed on PDI, the lysine variants and acetylated PDI. The enzymes structures were determined as well as the pKa of the cysteine residues at the active site were calculated.

### 3.12 Statistical analysis

The kinetic analysis was performed by fitting the data to the Michaelis-Menten equation:

$$v = \frac{V_{Max} \times [S]}{K_M + [S]}$$

Excel was used to fit the data to solve for the enzyme kinetic parameters,  $K_M$ , and  $V_{Max}$ . To determine statistical significance, an unpaired student t-test was used, where  $P < 0.05$  was taken as being statistically significant.

## Results

### 4.1 Reductase activity of PDI and PDI-Mutants, at physiological pH

Only one study has been conducted on the importance of the lysine residues flanking the active site (K57 and K401)(Kimura et al., 2004). This study suggested that these lysine residues play an important role for optimal PDI activity. Recently, our laboratory investigated the potential role of these lysine residues in the regulation of PDI activity, specifically through acetylation. Initially site-directed mutagenesis was performed on the lysine residues to obtain 9 different variants of PDI. The lysine residues at the active sites (K57 and K401) were either mutated individually or together to an alanine, glutamine, or glutamic acid (summarized in Table 1).

Before reductase assays were performed, the concentrations of enzymes were normalized through burst kinetics (Figure 6). The reaction consisted of Di-E-GSSG (800nM) and enzyme (10 $\mu$ L) in 100mM phosphate buffer (pH 7.4, 100 $\mu$ M DTPA). The increase of fluorescence was observed for 10 minutes, where the burst phase occurred in the first minute. The linear regression was obtained after the burst phase, where the y-intercept indicated the concentration of enzyme.

Steady-state kinetic parameters for the reductase activity of PDI and its lysine variants were determined by a fluorogenic assay using Di-E-GSSG as the substrate (50 nM – 4000 nM). The experiments were conducted at pH 7.4. A low concentration of DTT (10 $\mu$ M) was added to the buffer to reduce the enzyme. The baseline for the experiments was taken as the rate of reduction of Di-E-GSSG by DTT. The concentration of EGSH was calculated from a standard plot. The data for PDI and its lysine variants were fitted to the Michaelis-Menten equation (Figure 7). The Michaelis-Menten kinetic parameters ( $K_M$

<b>Protein</b>	<b><i>a</i> Domain</b>	<b><i>a'</i> Domain</b>
<b>wt-PDI</b>	<b>CGHCK</b>	<b>CGHCK</b>
<b>PDI K-Q <i>aa'</i></b>	<b>CGHCQ</b>	<b>CGHCQ</b>
<b>PDI K-Q <i>a</i></b>	<b>CGHCQ</b>	<b>CGHCK</b>
<b>PDI K-Q <i>a'</i></b>	<b>CGHCK</b>	<b>CGHCQ</b>
<b>PDI K-A <i>aa'</i></b>	<b>CGHCA</b>	<b>CGHCA</b>
<b>PDI K-A <i>a</i></b>	<b>CGHCA</b>	<b>CGHCK</b>
<b>PDI K-A <i>a'</i></b>	<b>CGHCK</b>	<b>CGHCA</b>
<b>PDI K-E <i>aa'</i></b>	<b>CGHCE</b>	<b>CGHCE</b>
<b>PDI K-E <i>a</i></b>	<b>CGHCE</b>	<b>CGHCK</b>
<b>PDI K-E <i>a'</i></b>	<b>CGHCK</b>	<b>CGHCE</b>

**Table 1.** A summary of all site-directed mutations performed on PDI. All K-E mutations were performed by Cody Caba in completion of his Honours Thesis research project.



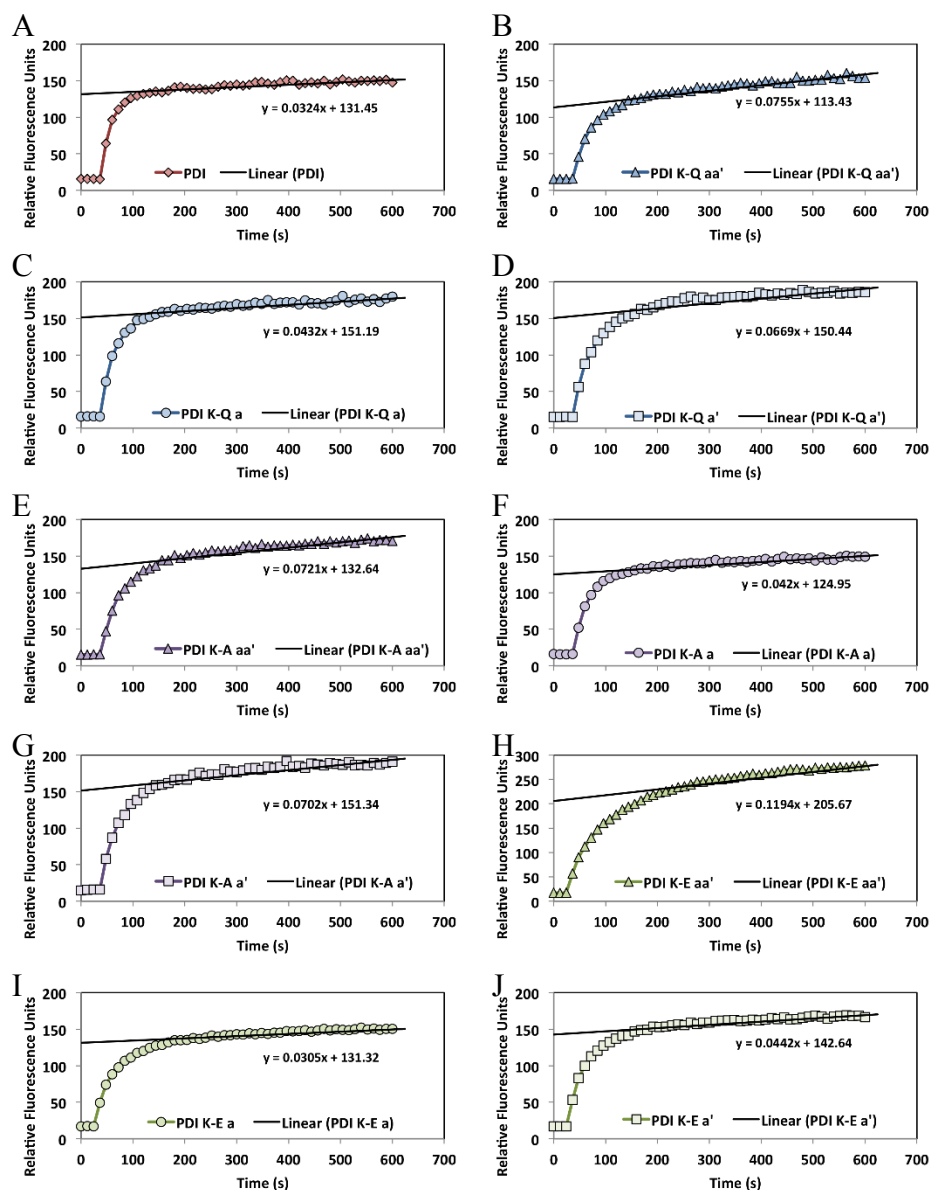


**Figure 6.** Burst kinetics for wt-PDI and mutants. For each experiment, 10  $\mu\text{L}$  of enzyme was reacted with 800 nM of Di-E-GSSG for 10 minutes. The linear regression was taken after the burst phase, where the y-intercept indicated the concentration of enzyme. All kinetics for K-E mutations (H, I, and J) were performed by Cody Caba as a part of his Honours Thesis research project.

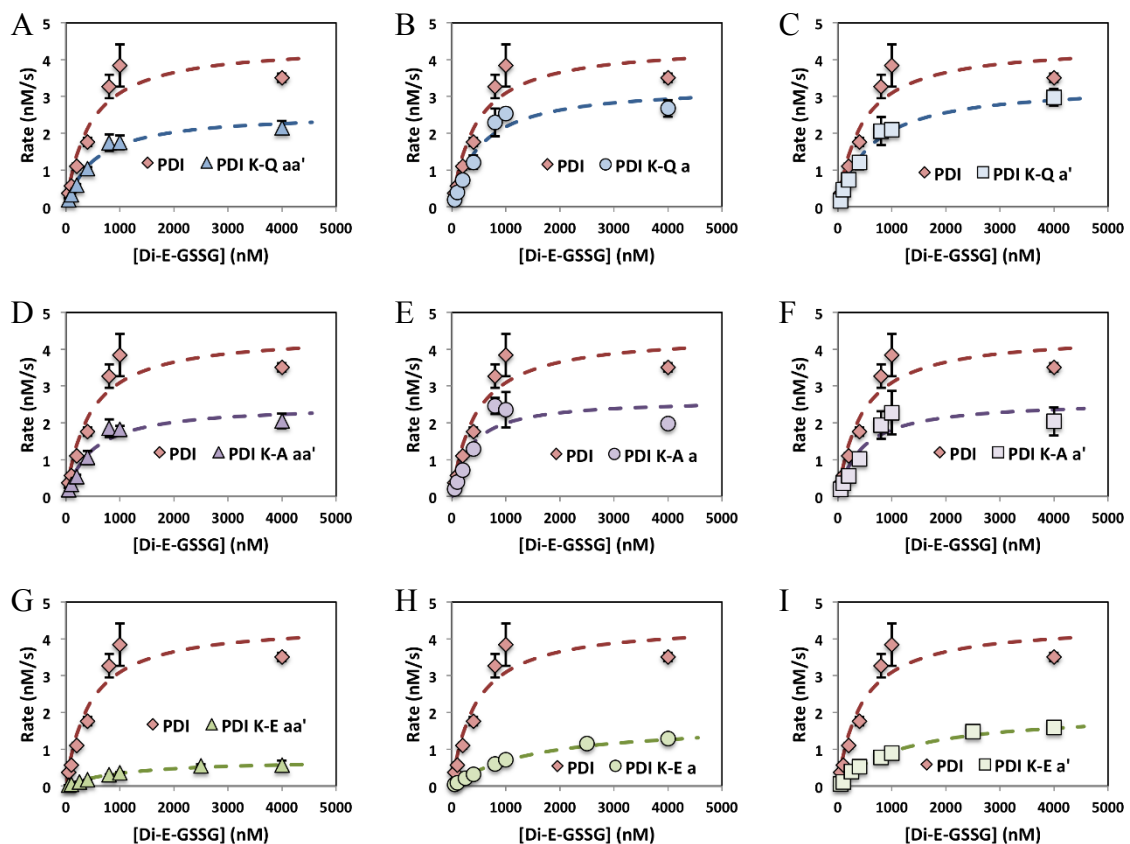


**Figure 7.** Initial rate vs. [Di-E-GSSG] plots for PDI and mutants. For each experiment the protein concentration was 20nM, and the initial rate was expressed as the amount of EGSH produced (nM/s). The assay was performed with 10 $\mu$ M of DTT in phosphate buffer (100mM phosphate pH 7.4, 0.1mM DTPA) and data was collected for 1 minute. The dashed lines represent the application of the best-fit kinetic parameters, obtained from the data, to the Michaelis-Menten equation. The error bars represent standard deviation, n=3. All kinetics for K-E mutations (G, H, and I) were performed by Cody Caba as a part of his Honours Thesis research project.

and  $V_{\text{Max}}$ ) and catalytic efficiency ( $k_{\text{cat}}/K_{\text{M}}$ ) were calculated for each protein and presented in (Figure 8). The reductase assay indicated that any mutation at either or both lysine residues (K57 and K401) results in a significant decrease ( $p < 0.05$ ) of  $V_{\text{Max}}$  (Figure 8C). The majority of mutants had a decrease of approximately 50% of wild type  $V_{\text{Max}}$ , where PDI K-E *aa'* had the lowest percentage of wild type  $V_{\text{Max}}$  at 17%. This indicates that a lysine residue provides maximum rate, and changing this residue to a negatively charged amino acid like glutamic acid will drastically decrease the rate of the enzyme. When comparing the  $K_{\text{M}}$  of wt-PDI with all the glutamine mutants and PDI K-A *a'* and *aa'* there was no significant difference observed ( $p < 0.05$ ) (Figure 8A). Interestingly, the  $K_{\text{M}}$  of PDI K-A *a* ( $333.04 \pm 5.043$  nM) was observed to be significantly lower ( $p < 0.05$ ) than wt-PDI ( $435.96 \pm 15.298$  nM). Due to the fact that the glutamic acid mutations would result in a reversal of charge from positive to negative it was not surprising that all glutamic acid mutants displayed a significantly higher ( $p < 0.05$ )  $K_{\text{M}}$  when compared to wild type. Interestingly, the catalytic efficiency for all lysine mutants was observed to be significantly lower ( $p < 0.05$ ) than wt-PDI ( $5.10 \pm 0.210 \times 10^5 \text{ M}^{-1}\text{s}^{-1}$ ) (Figure 8B). The mutant with the highest catalytic efficiency was PDI K-A *a* and PDI K-E *aa'* had the lowest catalytic efficiency. This further supports the notion that lysine is important for optimal reductase activity.

#### **4.2 The effect of the active site lysine residues on the pH optima of the reductase activity of PDI**

To further study the influence of active site lysine residues on PDI activity, a pH titration was performed. This was to specifically determine whether the positive charge

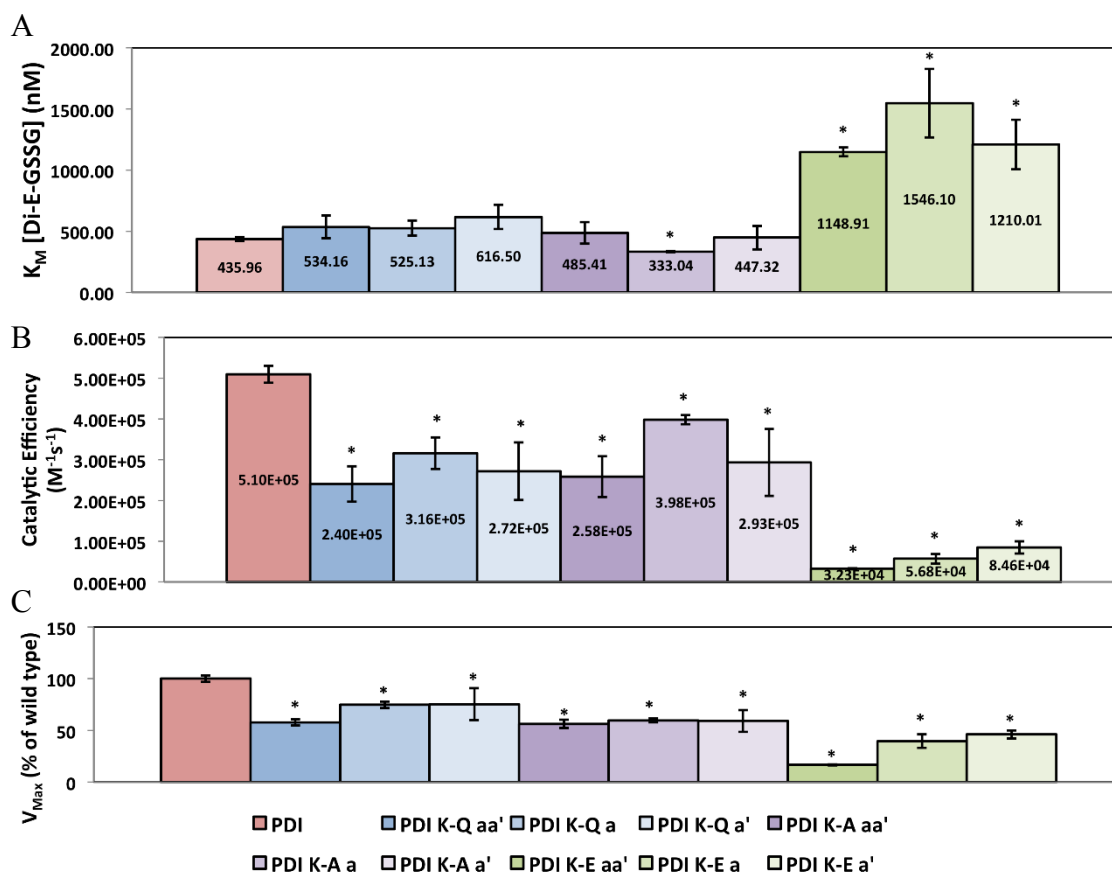


**Figure 8.** Michaelis-Menten kinetic parameters and catalytic efficiency ( $k_{cat}/K_M$ ) for wt-PDI and mutants at pH 7.4. The kinetic parameters and catalytic efficiency were estimated by utilizing a fit of the initial rate data of EGS<sub>H</sub> production by wt-PDI and the Lys variants by using the Solver function in MS Excel. Results are expressed as the mean with standard deviation,  $n=3$ . Significant differences ( $p<0.05$ ) are indicated by \*. All K-E mutation kinetics were performed by Cody Caba as a part of his Honours Thesis research project.

on the lysine residue affected the pKa of active site cysteine residues. For these experiments, Di-E-GSSG was kept constant at 400nM, and the pH was varied between 5.5 - 7.5. The initial rates at varying pH values were plotted for each set of amino acid mutant with wt-PDI (Figure 9). All of the lysine variants exhibited similar bell-shaped pH titration curves in comparison to wild type. It was observed that PDI reductase activity was most active at pH 6.5 and not physiological pH of 7.4 or the postulated pH of the ER, 7.2 (Wu et al., 2000). It was observed (Figure 9) that all proteins displayed bell-shaped curve where at pH 5.5 and 7.5 the initial rates were at their lowest, between  $0.5\text{nMs}^{-1}$  to  $1.5\text{nMs}^{-1}$ . Interestingly, wt-PDI and the lysine to glutamine and alanine variants all displayed similar initial rates at pH 6.

#### **4.3 Reductase activity of wt-PDI and PDI mutants, at pH 6.5**

Since pH 6.5 exhibited the highest initial rate for wt-PDI and all lysine variants (Figure 9) the fluorogenic reductase activity assays were repeated at pH 6.5. At this pH of 6.5, a higher percentage of lysine residues would be protonated resulting in a positive charge. Any possible acetylation of a lysine residue would neutralize the positive charge. The initial rates of EGSH production from Di-E-GSSG (25nM – 1000nM) were fitted to the Michaelis-Menten equation for wt-PDI and the lysine variants (Figure 10). The Michaelis-Menten kinetic parameters ( $K_M$  and  $V_{Max}$ ) and catalytic efficiency ( $k_{cat}/K_M$ ) were also calculated for each enzyme and presented in Figure 11. It was observed that almost all lysine variants displayed a reduction in  $V_{Max}$ , where only PDI K-Q *aa'* did not display a significant reduction ( $p < 0.05$ ) (Figure 11C). This further supports the notion that lysine is critical for optimal activity. The lysine variants displayed greater variability in

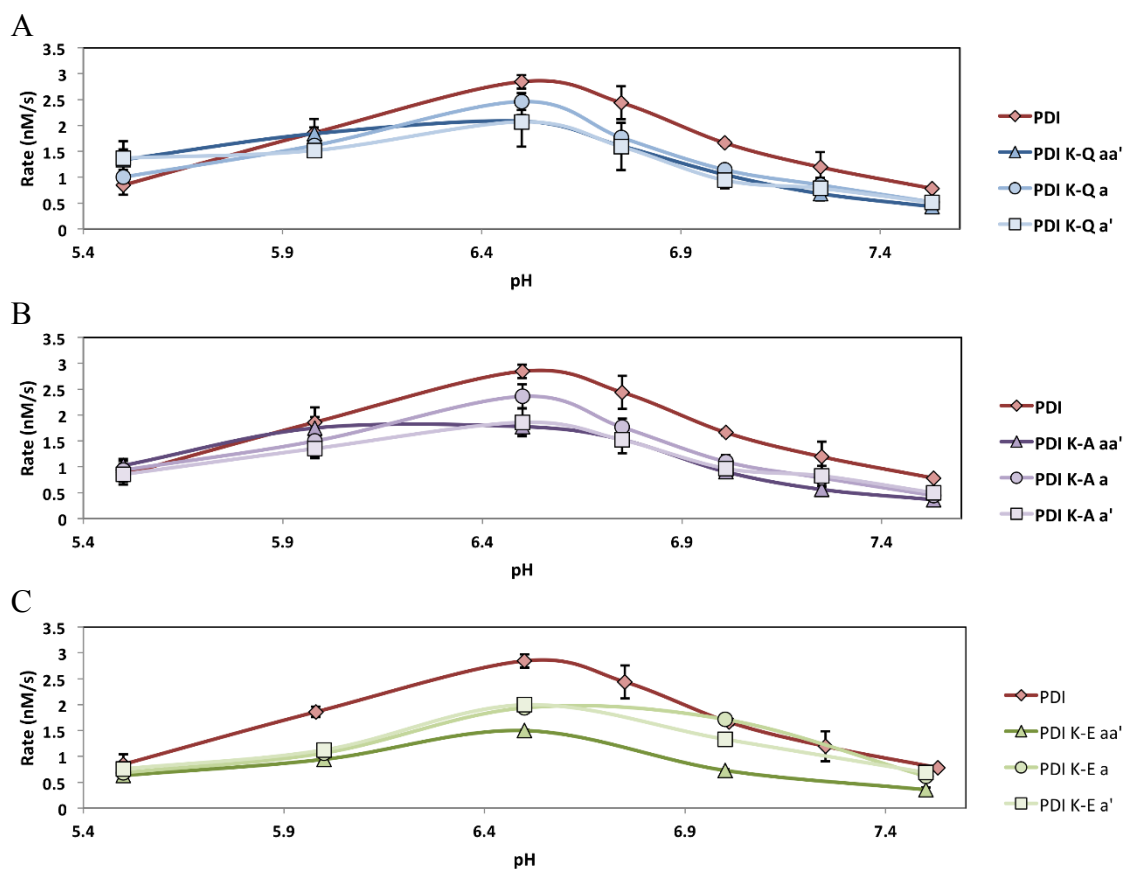


**Figure 9.** pH Titration curves of PDI and mutants. The concentration of wt-PDI was kept constant at 20nM and Di-E-GSSG was kept constant at 400nM. The change in pH occurred through the addition of NaOH. The rate was expressed as the amount of EGSH produced (nM/s). Results are expressed as the mean with standard deviation, n=3. All kinetics for K-E mutations (C) were performed by Cody Caba as a part of his Honours Thesis research project.

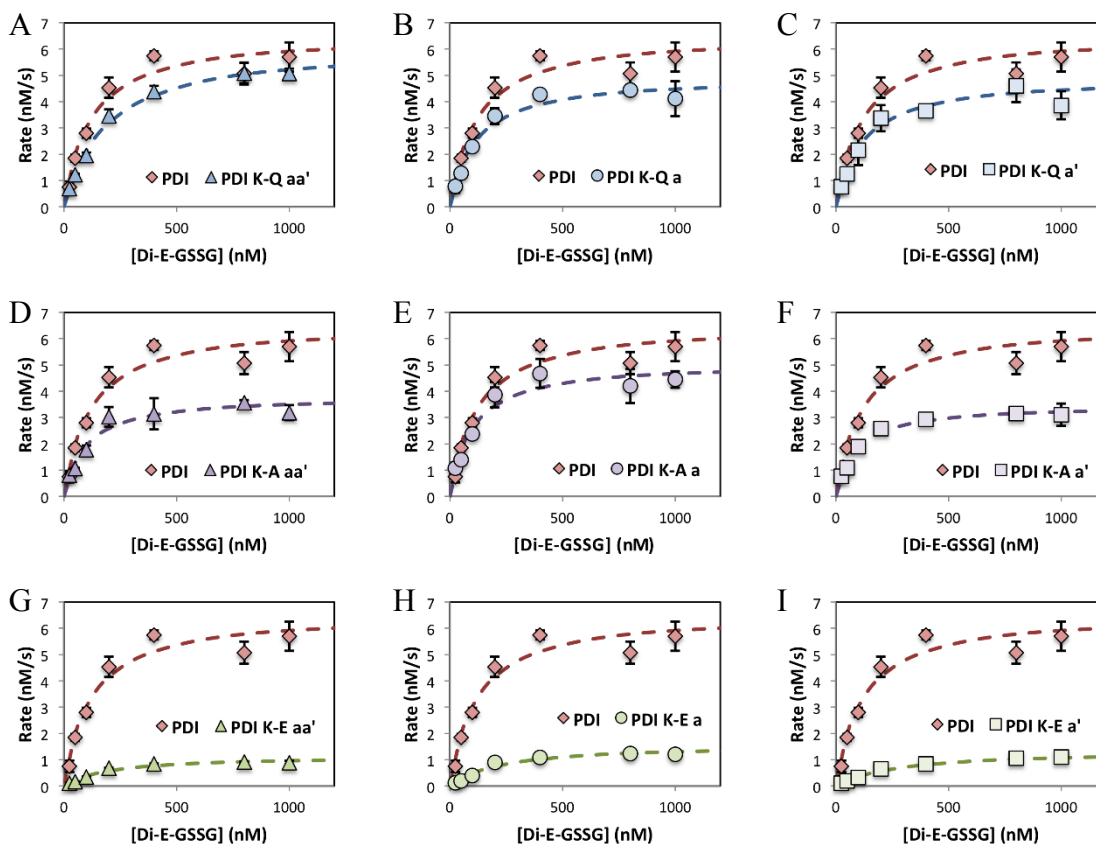


**Figure 10.** Initial rate vs. [Di-E-GSSG] plots for wt-PDI and mutants. For each experiment the protein concentration was 20nM, and the initial rate was expressed as the amount of EGSH produced (nM/s). The assay was performed with 10 $\mu$ M of DTT in phosphate buffer (100mM phosphate pH 6.5, 0.1mM DTPA) and data was collected for 1 minute. The dashed lines represent the application of the best-fit kinetic parameters, obtained from the data, to the Michaelis-Menten equation. The error bars represent standard deviation, n=3. All kinetics for K-E mutations (G, H, and I) were performed by Cody Caba as a part of his Honours Thesis research project.

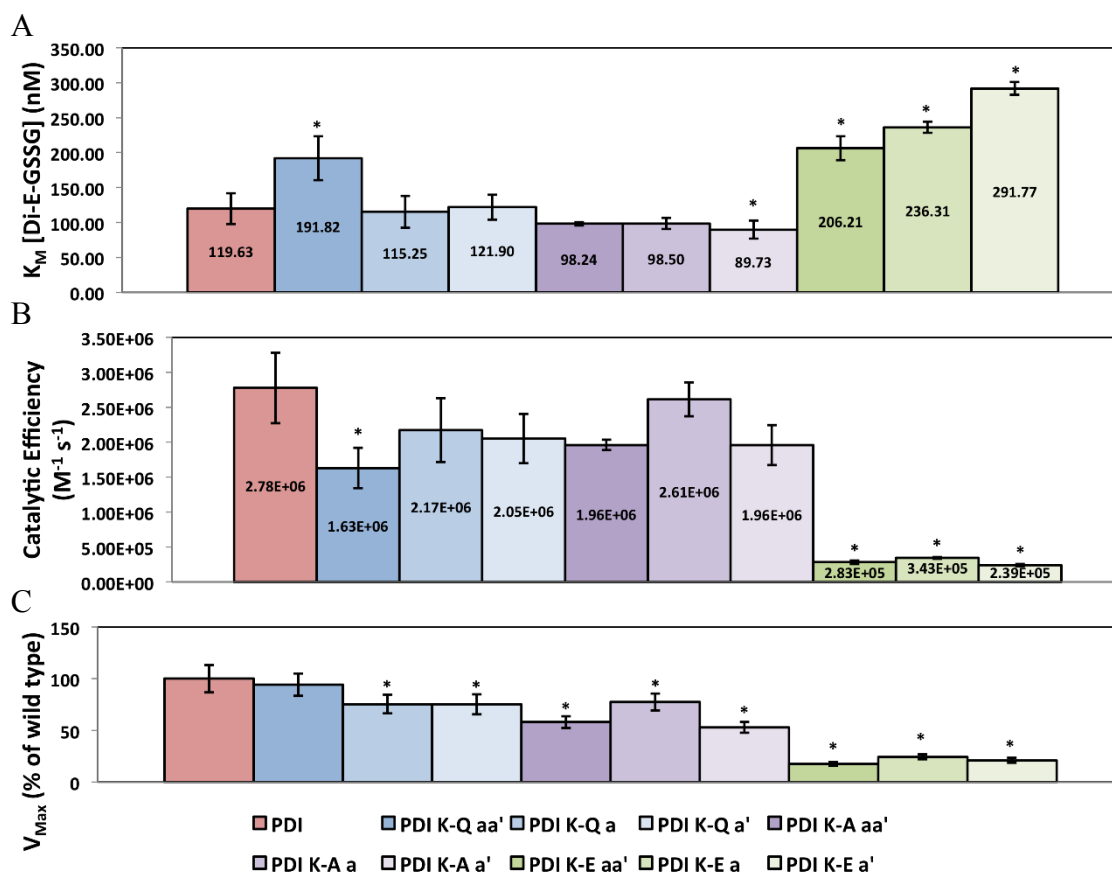


**Figure 11.** Michaelis-Menten kinetic parameters and catalytic efficiency ( $k_{cat}/K_M$ ) for wt-PDI and mutants. The kinetic parameters and catalytic efficiency were estimated from a fit of the initial rate data of EGSH production at pH 6.5 by wt-PDI and the Lys variants by using the Solver function in MS Excel. Results are expressed as the mean with standard deviation,  $n=3$ . Significant differences ( $p<0.05$ ) are indicated by \*. All K-E mutation kinetics were performed by Cody Caba as a part of his Honours Thesis research project.



$K_M$  when compared to wt-PDI ( $119.63 \pm 18.662$  nM) (Figure 11A). Interestingly, PDI K-Q *aa'* ( $191.82 \pm 31.416$  nM) showed a significant increase ( $p < 0.05$ ) in  $K_M$ . Also, as shown at pH 7.4, all lysine to glutamic acid variants exhibited significant increases ( $p < 0.05$ ) in  $K_M$ . This suggests that these lysine variants lower the binding affinity of the substrate to the protein. Interestingly, PDI K-A *a'* ( $89.73 \pm 12.866$  nM) exhibited a significant reduction ( $p < 0.05$ ) in  $K_M$  when compared to wt-PDI. Therefore, an alanine at the C-terminal end of the CXXC motif in the *a'* improves substrate binding. The catalytic efficiency of PDI was calculated to be  $2.78 \pm 0.506 \times 10^6$  M<sup>-1</sup>s<sup>-1</sup> (Figure 11B), which was higher than previously reported for PDI reductase activity (Raturi & Mutus, 2007). Only PDI K-Q *aa'*, PDI K-E *aa'*, PDI K-E *a*, and PDI K-E *a'* exhibited significantly lower ( $p < 0.05$ ) catalytic efficiency when compared to wt-PDI. This suggests these lysine variants reduce the protein's reductase activity, which further supports lysine as an integral residue for PDI activity.

#### 4.4 Computational structural and pKa analysis of active site cysteine residues

In collaboration with Dr. Gauld's Group, computational calculations were performed to estimate the pKa values for the active site cysteine residues (Li, Robertson, & Jensen, 2005) as a function of the lysine mutations. Computational analysis was performed on wt-PDI, the lysine variants, and on acetylated lysine residues (Table 2). The N-terminal cysteine residues in PDI displayed a lower pKa (C53 – 4.45, C397 – 4.66), whereas the C-terminal cysteine residues had a higher pKa (C56 – 8.67, C400 – 9.81). These results were comparable to previously reported values for the pKa of the cysteine residues (Karala et al., 2010; Nelson & Creighton, 1994). Interestingly, the acetylated *a* domain cysteine residues showed similar pKa values to those of PDI K-E *aa'*

<b>Protein</b>	<b>C53 pKa</b>	<b>C56 pKa</b>	<b>C397 pKa</b>	<b>C400 pKa</b>
<b>PDI</b>	<b>4.45</b>	<b>8.67</b>	<b>4.66</b>	<b>9.81</b>
<b>PDI K-Q aa'</b>	<b>4.96</b>	<b>8.52</b>	<b>4.06</b>	<b>8.16</b>
<b>PDI K-A aa'</b>	<b>4.39</b>	<b>12.98</b>	<b>4.83</b>	<b>12.58</b>
<b>PDI K-E aa'</b>	<b>5.43</b>	<b>10.43</b>	<b>4.78</b>	<b>8.29</b>
<b>PDI Acetylated (K57 and K401)</b>	<b>5.6</b>	<b>9.14</b>	<b>4.79</b>	<b>12.01</b>

**Table 2.** Computationally estimated pKa's of active site cysteines in the *a* and *a'* domain. Wanlei Wei of Dr. Gauld's group performed the computational analysis of all the proteins (Li et al., 2005).

in the *a* domain. Whereas, the acetylated *a'* domain cysteine residues showed similar pKa values to those of PDI K-A *aa'* in the *a'* domain. Through computational analysis, the structure of the *a'* domain active site was elucidated (Figure 12). The acetylated *a'* domain active site was also determined through dynamic simulations for comparison (Figure 13). It is noticeable from the acetylated active site that the lysine residue is shifted towards the backbone of the enzyme, whereas the un-acetylated lysine is pointed away from the active site cysteines. Also, it is noticeable that in the acetylated protein the cysteine residue (C400) is further away from the glutamic acid residue (E391).

#### **4.5 Identification of acetylated active site lysine residues through mass spectrometry**

The two active sites of PDI have similar sequences, which might be difficult to differentiate between the two using mass spectrometry. However, a previous study that used Glu-C as the protease for digestion was successful in identifying the two active sites (Kozarova et al., 2007). Therefore, a similar protocol was used, where PDI was proteolyzed by a 10:1 ratio of PDI to Glu-C. Digestion was performed overnight at room temperature. The double His-tagged PDI (60kDa) digests were desalted then analyzed by MALDI-TOF, and MS/MS was performed on active site parent ions for further confirmation (Figure 14). The expected mass-to-charge ratio ( $m/z$ ) for the active site fragments was 1692.8 (*a* domain) and 2462.2 (*a'* domain) as predicted by Protein Prospector software. Surprisingly, fragment peaks appeared at  $m/z$  1689.9 and 2459.6 and not at the predicted  $m/z$  (Figure 14A). However, through MS/MS these fragment were verified to be the active sites of PDI (Figure 14B and C).

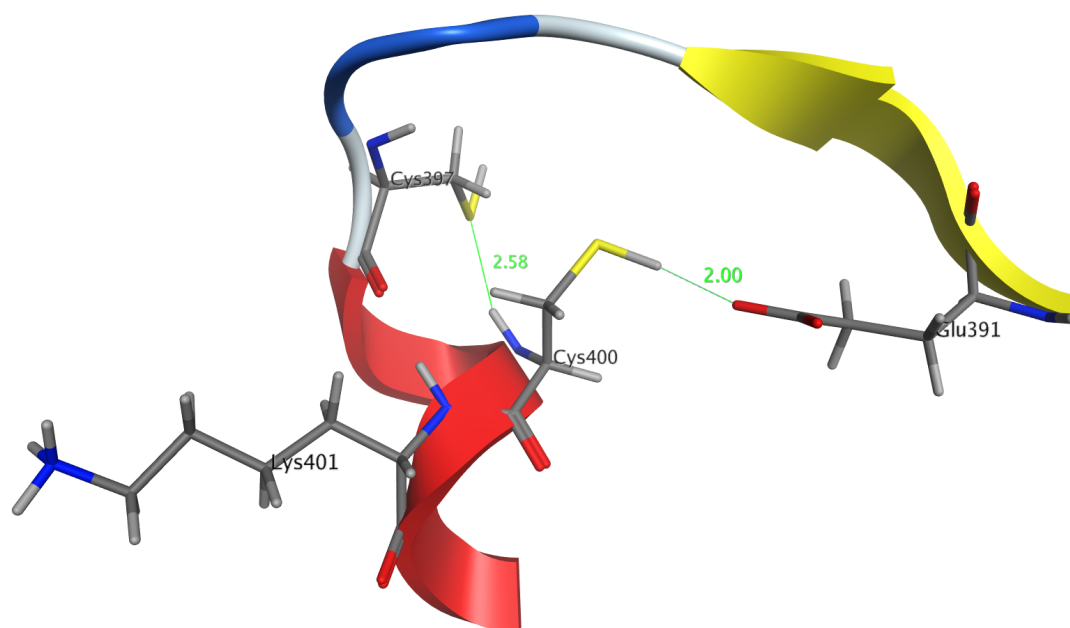


**Figure 12.** Computational dynamics simulation of wt-PDI  $\alpha'$  domain active site. Distances are provided in Angstroms. The atoms are represented by colours (yellow: sulfur, red: oxygen, blue: nitrogen, light grey: hydrogen, and dark grey: carbon). Wanlei Wei of Dr. Gauld's group performed the computational analysis of all the proteins.

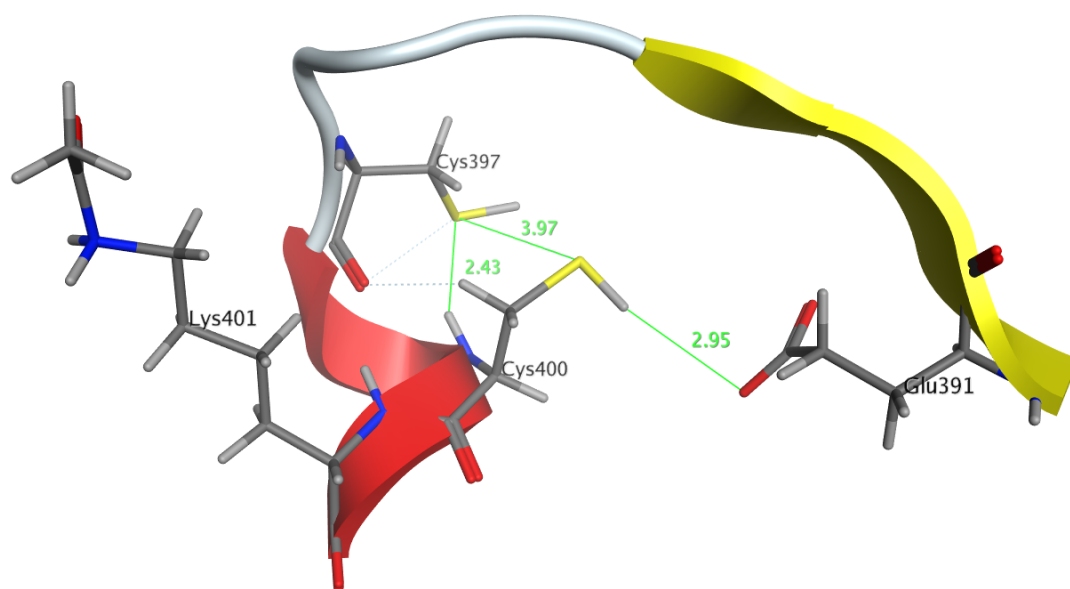


**Figure 13.** Computational dynamics simulation of acetylated wt-PDI  $\alpha'$  domain active site. Distances are provided in Angstroms. The atoms are represented by colours (yellow: sulfur, red: oxygen, blue: nitrogen, light grey: hydrogen, and dark grey: carbon). Wanlei Wei of Dr. Gault's group performed the computational analysis of all the proteins.

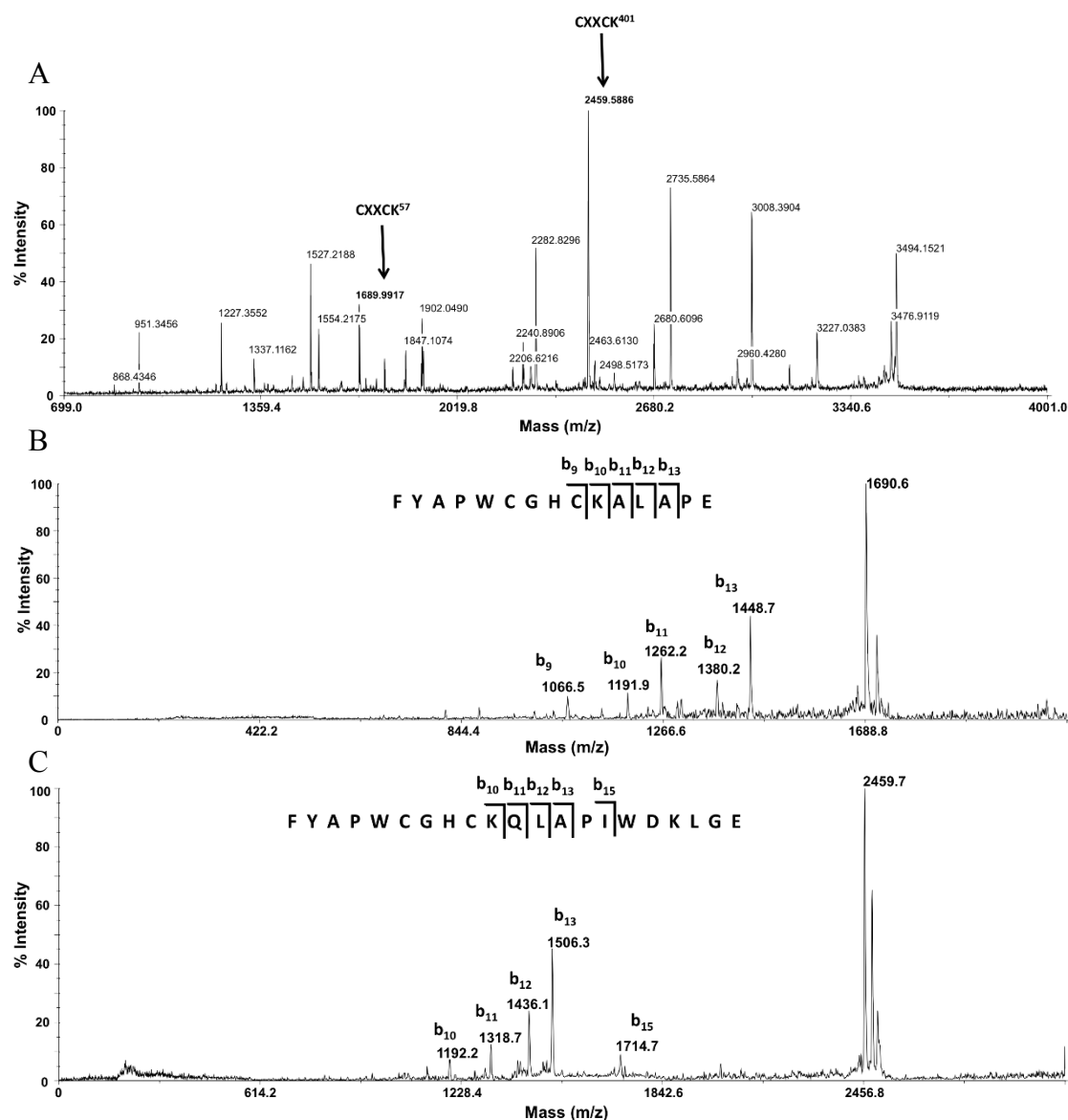


**Figure 14.** Mass fingerprint analysis of PDI Glu-C peptides. PDI digestion was performed overnight at room temperature using a 10:1 ratio of PDI to Glu-C. A) The mass fingerprint of PDI, where  $m/z$  1689 and 2459 corresponds to the active sites of PDI. B) The MS/MS of the  $m/z$  1689 parent ion corresponding to the *a* domain of PDI. C) The MS/MS of the  $m/z$  2459 parent ion corresponding to the *a'* domain of PDI.

An acetyltransferase (PCAF) was used to perform acetylation on PDI. PDI was reacted with PCAF and acetyl-CoA in a 1:2:20 ratio. After the reaction was incubated at 32°C for 2 hours, PDI was isolated using the His Select<sup>®</sup> Nickel Affinity column. PDI was then digested with Glu-C and analyzed on the MALDI-TOF. The active site fragment peaks were observed at  $m/z$  1690 and 2460 (Figure 15). However, no acetylated fragment peaks were observed, which would appear at  $m/z$  1734 and 2504.

Next, acetylation was performed chemically by acetic anhydride. PDI was reacted with acetic anhydride in a 1:10 ratio, for 2 hours at 37°C. PDI was desalted to remove excess acetic anhydride and digested with Glu-C. The fragments were analyzed on the MALDI-TOF. The active site fragment peaks were again observed at  $m/z$  1691 and 2459 (Figure 16A). An acetylation peak was observed as well at  $m/z$  2502, which is a 42Da increase of the 2459 peak indicative of acetylation. This peak was further analyzed and confirmed through MS/MS to be the acetylated  $\alpha'$  domain (Figure 16B). The MS/MS suggests that lysine 401 has been acetylated by the presence of the  $b_{10}$  ion. This indicates that the  $\alpha'$  domain active site lysine of PDI appears to be partially acetylated due to the presence of both un-acetylated and acetylated peptides.

#### **4.6 Reductase activity of un-acetylated and acetylated PDI and PDI K-Q $\alpha\alpha'$**

Chemical acetylation of PDI and PDI K-Q  $\alpha\alpha'$  was performed using acetic anhydride. Acetylation was performed for 2 hours at 37°C, where after incubation the protein was desalted. The fluorogenic reductase assay Di-E-GSSG (25nM-1000nM) was performed at pH 6.4 in phosphate buffer. The initial rates of EGSH production were fitted to the Michaelis-Menten equation for both un-acetylated and acetylated protein (Figure 17). The Michaelis-Menten kinetic parameters ( $K_M$  and  $V_{Max}$ ) and catalytic efficiency

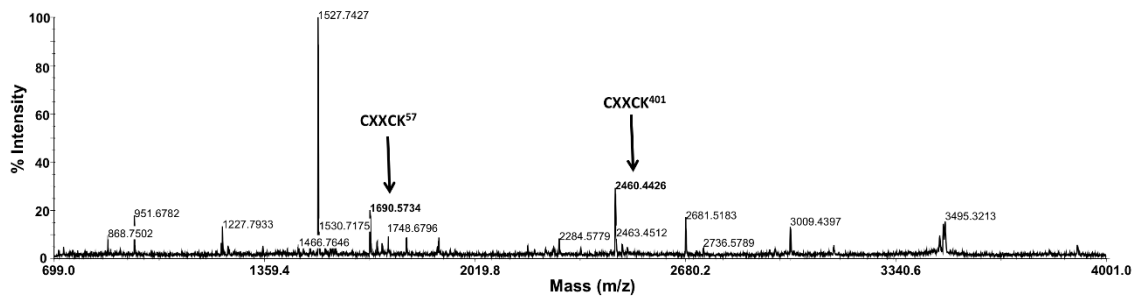


**Figure 15.** Mass fingerprint analysis of PDI reacted with acetyltransferase (PCAF). PDI was incubated with PCAF and acetyl-CoA for 2 hours at 32°C. PDI was digested with Glu-C overnight at room temperature. Only the un-acetylated peptide fragments are observed in the mass fingerprint.



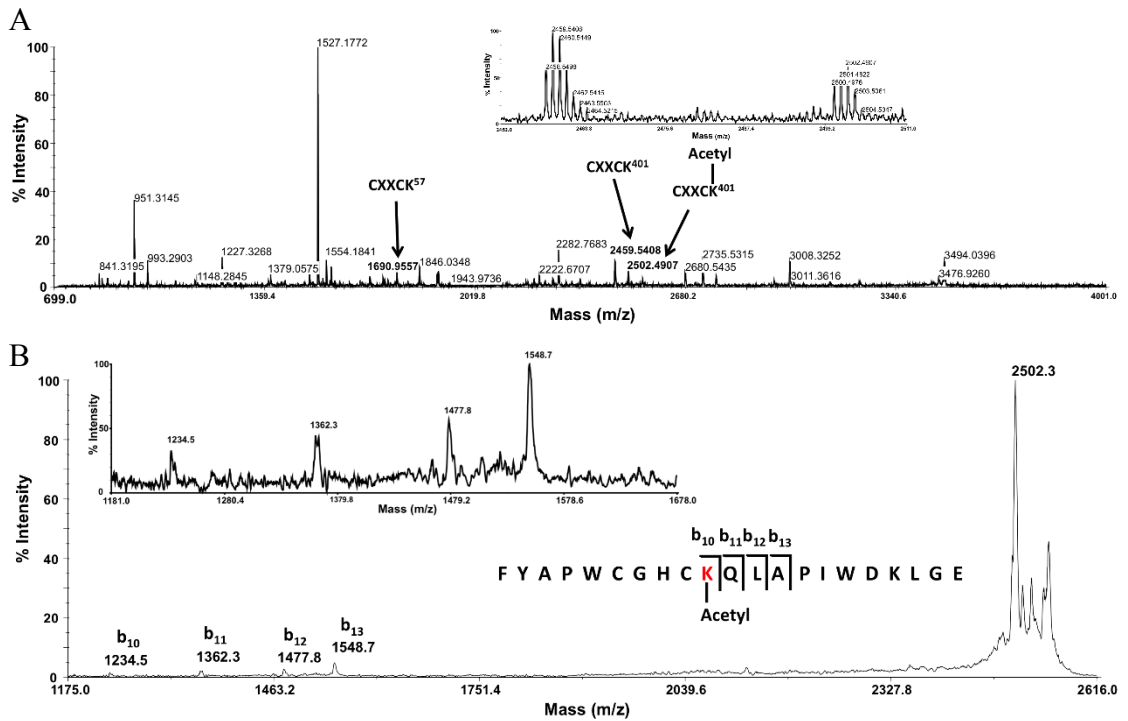


**Figure 16.** Mass fingerprint analysis of PDI reacted with acetic anhydride. PDI was incubated with acetic anhydride for 2 hours at 37°C. PDI was then digested with Glu-C overnight at room temperature. A) Un-acetylated peptide fragments are observed in the mass fingerprint. The *a'* active site domain is observed to be acetylated with a *m/z* 2502. B) The MS/MS of the *m/z* 2502 parent ion, which corresponds to the acetylated active site *a'* domain.

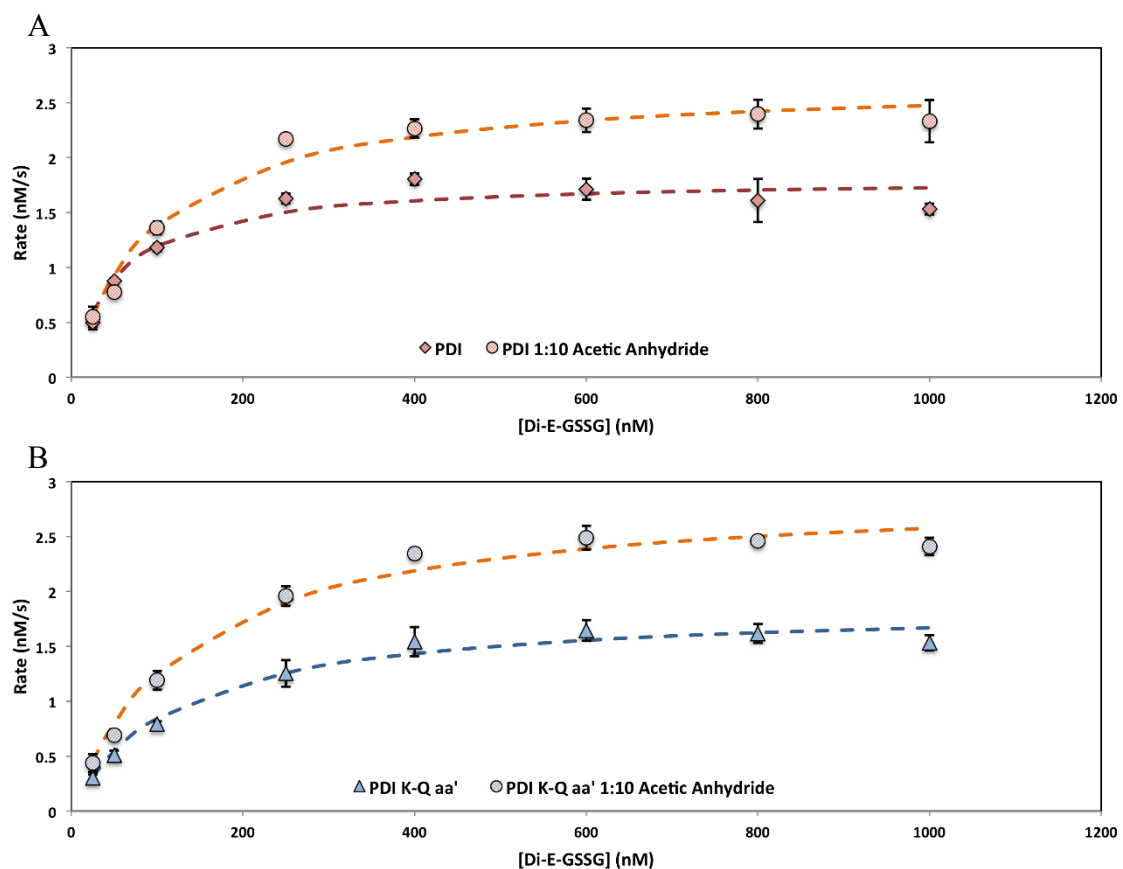


**Figure 17.** Initial rate vs. [Di-E-GSSG] plots for un-acetylated and acetylated wt-PDI and PDI K-Q *aa'*. For each experiment the protein concentration was 20nM, and the initial rate was expressed as the amount of EGSH produced (nM/s). The assay was performed with 10 $\mu$ M of DTT in phosphate buffer (100mM phosphate pH 6.5, 0.1mM DTPA) and data was collected for 1 minute. The dashed lines represent the application of the best-fit kinetic parameters, obtained from the data, to the Michaelis-Menten equation. The error bars represent standard deviation, n=3.

( $k_{cat}/K_M$ ) were calculated and presented in (Figure 18). Interestingly, the  $V_{Max}$  of acetylated PDI and PDI K-Q *aa'* both significantly increased ( $p<0.05$ ) indicating that acetylation may increase the turnover rate (Figure 18C). However, for  $K_M$  only the acetylation of wt-PDI resulted in a significant increase ( $p<0.05$ ) (Figure 18A). Whereas, acetylated compared to un-acetylated PDI K-Q *aa'* produced no significant change in  $K_M$ . This indicates that the acetylation at the active site lysine results in a decrease in affinity to the substrate. Interestingly, acetylated wt-PDI was observed to significantly decrease ( $p<0.05$ ) catalytic efficiency in comparison to un-acetylated (Figure 18B). Whereas, acetylated PDI K-Q *aa'* was observed to significantly increase ( $p<0.05$ ) catalytic efficiency in comparison to un-acetylated. This suggests that acetylation at the active lysine may inhibit the reductase activity, whereas acetylation at other lysine residues may increase the reductase activity.

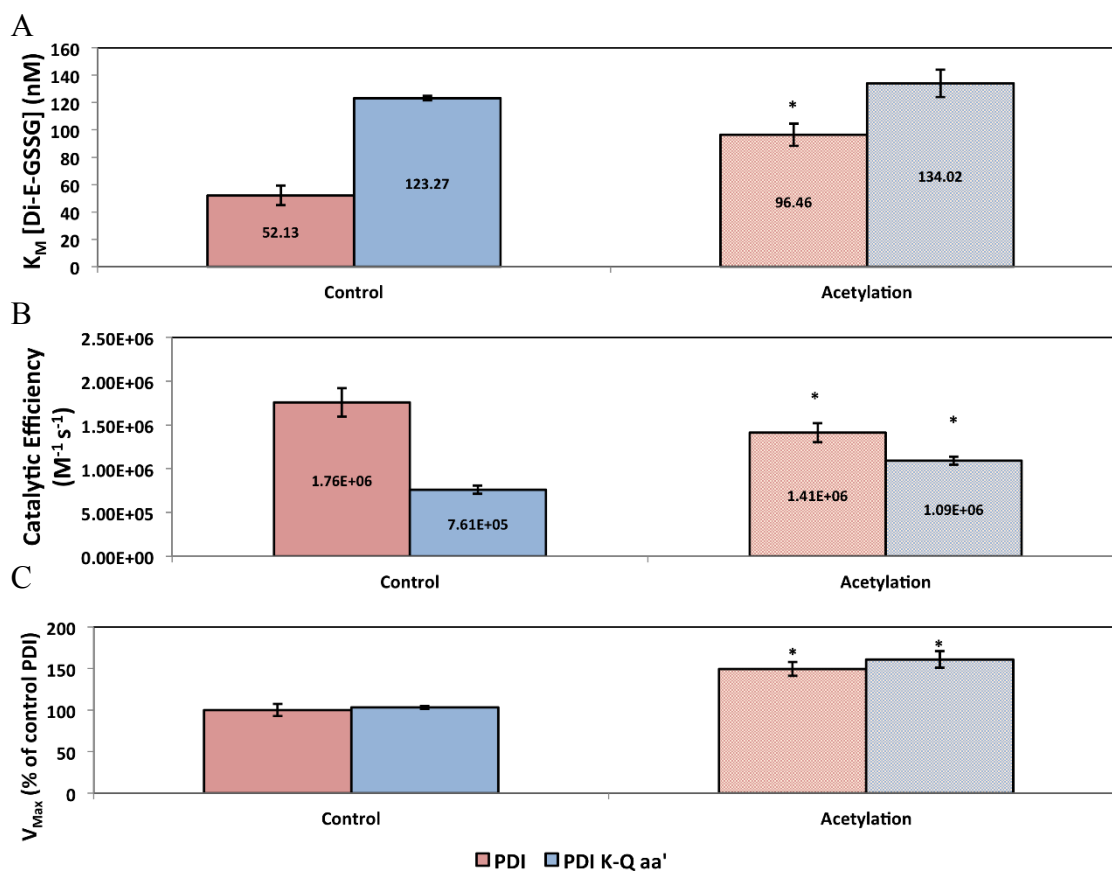


**Figure 18.** Michaelis-Menten kinetic parameters and catalytic efficiency ( $k_{cat}/K_M$ ) for wt-PDI and mutants. The kinetic parameters and catalytic efficiency were estimated from a fit of the initial rate data of EGSH production at pH 6.5 by wt-PDI and the Lys variants by using the Solver function in MS Excel. Results are expressed as the mean with standard deviation,  $n=3$ . Significant differences ( $p<0.05$ ) are indicated by \*.

## Discussion

### 5.1 The importance of active site-flanking lysine residues in the reductase activity of PDI

Lysine residues play an important role to maintain protein structure and function, through hydrogen bonds or electrostatic interactions (Patel et al., 2011). The role of PDI active site-flanking lysines has not been well studied. In fact there is only one study to our knowledge, which has been conducted on the importance of this residue in PDI (Kimura et al., 2004). In the earlier study, the researchers mutated away the cysteine residues in the  $\alpha'$  domain and focused on the lysine in the  $\alpha$  domain (Kimura et al., 2004). The lysine residue in the  $\alpha$  domain was then mutated to glutamine and arginine, where a decrease in activity was observed (Kimura et al., 2004). The assay used in this study involved the reduction of insulin by PDI, which was monitored by spectrophotometry. However, this study or any other studies to our knowledge have not delved into how lysine residues affect the redox activity of PDI as well as how they may be used to regulate PDI activity.

In the current study, lysine residues (K57 and K401) were mutated individually or together to further investigate the role lysine plays at both the  $\alpha$  and  $\alpha'$  domains. The lysine residues were mutated to glutamine, alanine, or glutamic acid (Table 1). Glutamine was chosen for the reason that it can form hydrogen bonds as well as it best mimics the bulky characteristics of lysine while it provides a neutral charge. Lysine was mutated to glutamic acid in order to observe the effects of PDI activity with a negative charge taking the place of the positively charged of lysine residue. A small neutral amino acid such as alanine was chosen to observe if flexibility at that site provides any change in activity of

PDI. These mutations will provide further understanding of the role of lysine at the active site of PDI.

The steady-state kinetic parameters observed at pH 7.4 provided vital information of how lysine may play a role in PDI reductase activity (Figure 8). The  $K_M$  of most lysine variants showed very little change in comparison to wt-PDI ( $435.96 \pm 15.298$  nM). This indicates that these mutations did not affect the binding of substrate to the enzyme. In the case of the PDI K-A  $\alpha$  domain, surprisingly displayed a significant decrease in  $K_M$  ( $333.04 \pm 5.043$  nM). This suggests that a more flexible amino acid at the  $\alpha$  domain may improve the accessibility of the substrate to the active site. However, all the glutamic acid mutants demonstrated a significant increase in  $K_M$  (Figure 8A). This may suggest that a negative charge near the active site inhibits the initial binding of the substrate to the active site.

It was observed that all lysine variants displayed a significant decrease in  $V_{Max}$  (Figure 8C). This suggests that any neutral or negatively charged amino acid will hinder the turnover rate of the enzyme. Interestingly, as previously stated (Table 2), the  $pK_a$  of the two cysteines in the active site are quite different. The N-terminal cysteine is observed to have a  $pK_a$  around 4, which is hypothesized to form a thiolate and bind to the substrate (Karala et al., 2010). The C-terminal cysteine is observed to have a  $pK_a$  around 9, and it is hypothesized that the  $pK_a$  of this cysteine will decrease in order to form a thiolate and release the substrate from the N-terminal cysteine (Nelson & Creighton, 1994). From the  $V_{Max}$  results, it is apparent that lysine plays a significant role in turnover rate, where we postulate that the positive charge on the lysine may help reduce the  $pK_a$  of the C-terminal cysteine. The fact that all glutamic acid mutants demonstrated the lowest

$V_{\text{Max}}$  values support this theory that the positive charge on lysine may help to reduce the  $pK_a$  of the C-terminal cysteine. The catalytic efficiency of the lysine variants were all significantly lower than wt-PDI (Figure 8B). This suggests that lysine is needed for optimal PDI activity.

In order to observe the effect that the lysine variants have on the  $pK_a$  of the cysteine residues, a pH titration was performed (Figure 9). Surprisingly, none of the lysine variants caused a shift in the pH titration curve. All enzymes created a bell-like curve, where PDI and all the lysine variants were most active at pH 6.5 (Figure 9).

Therefore, the steady-state kinetics on PDI and the lysine variants were repeated at pH 6.5 (Figure 11). The kinetic parameters at pH 6.5 displayed some differences to the kinetic parameters observed at pH 7.4. PDI K-Q *aa'* displayed a significant increase in  $K_M$ , suggesting that Di-E-GSSG was inhibited from reaching the active site (Figure 11A). This could be due to the fact that glutamine residues at the lower pH form more hydrogen bonding and therefore results in a less accessible active site. Interestingly, at pH 7.4 PDI K-A *a* (Figure 8A) demonstrated a lower  $K_M$ . However, at pH 6.5 it is PDI K-A *a'* that exhibited a significant decrease in  $K_M$  (Figure 11A). This could possibly suggest that a change in pH would change which domain is more active. As previously observed at pH 7.4, glutamic acid mutants exhibited a significantly higher  $K_M$  than wt-PDI at pH 6.5 (Figure 11A).

Unexpectedly, PDI K-Q *aa'* exhibited no significant change in  $V_{\text{Max}}$  compared to wt-PDI (Figure 11C). It is possible that the increase in hydrogen bonding at the lower pH resulted in a more rigid structure where the cysteine residues would more easily form thiolates. This would result in a turnover rate that is larger than expected. All other lysine

variants exhibited a significant decrease in  $V_{\text{Max}}$  at pH 6.5 as previously seen at pH 7.4 (Figure 8C and Figure 11C). PDI K-Q *aa'* and all the glutamic acid mutants displayed a significantly lower catalytic efficiency compared to wt-PDI at pH 6.5 (Figure 11B). However, the other lysine variants did not appear to have a significantly lower catalytic efficiency compared to wt-PDI at pH 6.5 (Figure 11B). This could suggest that at a lower pH, the efficiency of the enzyme is not fully predicated on a lysine residue being at the active site. However it should be noted that wt-PDI ( $2.78 \pm 0.506 \times 10^6 \text{ M}^{-1}\text{s}^{-1}$ ) still exhibited the highest catalytic efficiency and is higher than previously reported for reductase activity (Raturi & Mutus, 2007).

## 5.2 The possible regulation of PDI by lysine acetylation

Recently, more extensive studies have been conducted in regards to lysine acetylation; specifically on non-histone acetyltransferases (Marmorstein, 2004). Now, it is understood that acetylation may play a role on an increasing number of proteins throughout the cell (Pehar & Puglielli, 2013). In the recent proteomic study of all ER acetylated proteins, PDI was observed to be acetylated, indicating the possible role as a post-translation modification to regulate PDI activity (Pehar et al., 2012). It was observed that PDI contains 7 sites of acetylation on PDI (Table 3) (Pehar et al., 2012). Interestingly, the lysine residue flanking the active site at the *a'* domain (K401) was acetylated (Table 3)(Pehar et al., 2012). This further confirmed that the active site-flanking lysine residues may act as a possible regulator of PDI activity.

Through computational analysis performed by Dr. Gauld's group, the pKa's of the cysteine residues at the active site were determined for the lysine variants as well as for acetylated lysine residues (K57 and K401) on PDI (Table 2). The calculations revealed



<b>PDI Domain</b>	<b>Sequence</b>
<i>b</i> ' domain	IKPHLMSQELPEDWDKQPVK
<i>a</i> ' domain	NVFVEFYAPWCGHCKQLAPIWDKLGETYK
<i>b</i> ' domain	ILEFFGLKK
<i>a</i> ' domain	NFEDVAFDEKK
<i>a</i> ' domain	DHENIVIAKMDSTANEVEAVK

**Table 3.** Sequences of acetylated peptides found in PDI through mass spectrometry. Lysine residues in red font indicate acetylated residue. Information taken from supplementary data of Pehar, M. et al. (2012). *Journal of Biological Chemistry*, 287(27).

that a mutation or acetylation of those lysine residues would result in a change in  $pK_a$  of the active site cysteine residues (Table 2). This suggested that the lysine plays an important role in maintaining the correct microenvironment for the cysteine residues. By changing the charge as well as creating a bulkier group on lysine resulted in a change in the microenvironment. It should be noted that acetylation of a lysine and glutamine, which both contain a carbonyl group, could be an acceptor for hydrogen bonding.

Interesting changes occurred in the molecular dynamic simulations of the un-acetylated and acetylated wt-PDI (Figure 12 and Figure 13). From the un-acetylated wt-PDI (Figure 12) it was evident that the lysine residue (K401) was positioned away from the active site of PDI. In the acetylated wt-PDI (Figure 13), the acetyl-lysine was shifted towards the backbone of the active site. This could be caused by a potential hydrogen bond between the carbonyl group of the acetyl moiety and the amino group of the backbone. Interestingly, the C-terminal cysteine residue was observed to be in very close proximity to a glutamic acid residue (E391). This could be the cause of the increase in  $pK_a$  of the C-terminal cysteine (Table 2), since a negatively charged residue will influence the sulfur to be in a protonated state. In this reduced conformation of wt-PDI, likelihood of reactive thiolate formation at the C-terminal cysteine would be decreased. This further supports that substrate would bind to the N-terminal cysteine causing a conformational change, which would result in the lowering of the  $pK_a$  of the C-terminal cysteine.

In the acetylated wt-PDI it was observed that the C-terminal cysteine is further away from the glutamic acid residue by almost an Å of distance. This suggests that the cysteine residue (C400) would have a lower  $pK_a$  due to the fact that the sulfur is further

away from a negative charge. However, though the computational analysis of the pKa's (Table 2), it was observed that the  $\alpha'$  domain C-terminal cysteine (C400) had an increase in pKa. This was a surprising observation and suggests that further investigation is required to understand how the C-terminal cysteine residue possesses a high pKa while still maintaining reactivity. This also suggests that acetylation of the lysine residue (K401) would result in a decrease in turnover rate of PDI because of the high pKa of the C-terminal cysteine.

To further understand the affects of lysine acetylation on PDI, *in vitro* acetylation was first performed by an acetyltransferase (PCAF). However, through mass spectrometry it was determined that PDI was not acetylated by this enzyme (Figure 15). PCAF is an acetyltransferase that is part of the GNAT family and is found primarily in the nucleus (Gupta, Samant, Smith, & Shroff, 2008). The use of PCAF as an acetyltransferase was based on the fact that it was accessible. It was assumed that the acetylation of PDI by this acetyltransferase was unlikely to occur.

Since PCAF was not successful, a cruder acetylation process was performed using acetic anhydride. This procedure has the potential non-specific acetylation of lysine residues. When a 10:1 ratio of acetic anhydride to PDI was reacted, it was observed that PDI became acetylated through mass spectrometry (Figure 16). The  $\alpha'$  domain was confirmed to be acetylated through MS/MS of the  $m/z$  2501 parent ion. The presence of a 42Da increase in the  $b_{10}$  ion from the un-acetylated PDI in comparison to the acetylated PDI confirmed the presence of acetylation on the active site-flanking lysine residue (K401) (Figure 14C and Figure 16B). However, it should be noted that the  $\alpha'$  domain flanking lysine (K401) was not fully acetylated due to the presence of the  $m/z$  2459

(Figure 16A). Therefore, through mass spectrometry analysis it was determined that PDI became partially acetylated by acetic anhydride and not by the acetyltransferase PCAF.

Steady-state kinetics were performed on un-acetylated and acetylated wt-PDI and PDI K-Q *aa'* at pH 6.5 (Figure 17). PDI K-Q *aa'* was used in addition to wt-PDI because the amino acid glutamine more closely resembles lysine and the glutamine would not be acetylated by acetic anhydride. The  $V_{\text{Max}}$  of the acetylated enzymes displayed significant increases in comparison to the un-acetylated enzymes (Figure 18C). The fact that acetylation of both wt-PDI and PDI K-Q *aa'* caused an increase, suggests that acetylation of PDI at lysine residues that are not flanking the active site may assist in enzyme turnover rate. This is a surprising result since the  $pK_a$  analysis suggested that acetylation at the active site-flanking lysine residue would result in an increase in  $pK_a$  and in effect decrease the turnover rate of the enzyme. However, it appears that acetylation at other lysine residues overwhelms the predicted inhibitory effect that the acetylated lysine at the active site provides.

Interestingly, the  $K_M$  of acetylated wt-PDI ( $96.46 \pm 8.236$  nM) significantly increased in comparison to the un-acetylated wt-PDI ( $52.13 \pm 7.221$  nM) (Figure 18A). Whereas, there was no significant change in  $K_M$  for acetylated PDI K-Q *aa'* and unacetylated PDI K-Q *aa'* (Figure 18A). This possibly suggested that acetylation at the active site-flanking lysine residues, specifically the *a'* domain resulted in a decrease in substrate binding to the active site. The fact that acetylated PDI K-Q *aa'* did not change significantly compared to un-acetylated PDI K-Q *aa'*, suggests that acetylation at other lysine residues did not affect substrate binding to the enzyme.

The catalytic efficiency of acetylated wt-PDI ( $1.41 \pm 0.110 \times 10^6 \text{ M}^{-1}\text{s}^{-1}$ ) was significantly reduced in comparison to un-acetylated wt-PDI ( $1.76 \pm 0.163 \times 10^6 \text{ M}^{-1}\text{s}^{-1}$ ) (Figure 18B). However, acetylated PDI K-Q *aa'* ( $1.09 \pm 0.048 \times 10^6 \text{ M}^{-1}\text{s}^{-1}$ ) resulted in a significant increase in catalytic efficiency in comparison to un-acetylated PDI K-Q *aa'* ( $7.61 \pm 0.471 \times 10^5 \text{ M}^{-1}\text{s}^{-1}$ ) (Figure 18B). Interestingly, acetylation at the flanking active site lysine residues may inhibit PDI activity through the inhibition of substrate binding and not through the inhibition of product release. However surprisingly, PDI activity surprisingly increased when acetylated at non-active site-flanking lysine residues, by promoting the turnover rate.

It should be noted that acetylation by acetic anhydride may not reproducibly acetylate the same lysine residue. This implies that these acetylation results should be evaluated cautiously when making any implications into how acetylation affects PDI. These acetylation experiments should be repeated to observe if reproducible. Also, since wt-PDI was only partially acetylated by acetic anhydride at lysine residue 401, it could be appropriate to repeat the experiments using an increased concentration of acetic anhydride to fully acetylate the enzyme at the active site lysine. To accurately draw conclusions about the role of acetylation on PDI, the reproducibility of this protocol must be confirmed.

## Conclusion

The investigation into the role of PDI active site-flanking lysine residues suggests that these lysine residues assist in PDI redox activity. The rationale behind this is that all lysine variants, with the exception of PDI K-Q aa', resulted in a decrease in  $V_{\text{Max}}$ . PDI K-Q aa' did not exhibit a significant decrease in  $V_{\text{Max}}$  at pH 6.5, however it did exhibit this at pH 7.4 (Figure 8C and Figure 11C). Additionally, the catalytic efficiency of all lysine variants significantly decreased at pH 7.4 (Figure 8C). At pH 6.5 all lysine variants had a decrease in catalytic efficiency, however only a few showed significant decrease (Figure 11C). This suggests that active site-flanking lysine residues may play greater of a role in the release of product and possibly the regeneration of enzyme than in substrate binding.

Mutating the lysine residue to glutamic acid, resulted in a charge change for the residue from positive to negative. From the kinetic assays at both pH 7.4 and 6.5, it is observed that the change in charge greatly affects the redox activity of PDI (Figure 8 and Figure 11). The catalytic efficiency of the enzyme is greatly reduced by the presence of the negative charge incurred by the glutamic acid (Figure 8C and Figure 11C). This suggests a post-translation modification such as succinylation, which causes a change in charge to lysine would have a greater effect on PDI redox activity (Zhang et al., 2011). Further studies into succinylation of PDI should be conducted, due to the fact that this much larger and negatively charged modification would affect PDI redox activity greatly.

Conclusions drawn from the acetylation of PDI by acetic anhydride should be considered cautiously as previously stated. However, the kinetic assay possibly suggests that acetylation of the active site-flanking lysine residue could adversely affect substrate binding (Figure 18A). Although, acetylation at non-active site lysine residues may

actually result in an improvement of product release from the enzyme (Figure 18C). Due to the fact that there is a study demonstrating that acetylation occurs on PDI, additional research is required to further understand the consequences of this post-translational modification.

To further study the relationship of acetylation on PDI's redox activity, one could possibly obtain acetyltransferases present in the ER to perform acetylation. Such acetyltransferases are ATase 1 and ATase 2, which belong to the GNAT superfamily (Pehar & Puglielli, 2013). Performing acetylation *in vitro* would be the simplest method to obtain improved valid results on the regulation of PDI by acetylation. To further study the effects of lysine acetylation, *in vivo* experiment should be conducted to obtain the most accurate lysine acetylation of PDI. In all these future experiments acetylated PDI should be isolated from un-acetylated PDI using antibodies for acetylation. These experiments would provide a more accurate account for how acetylation would regulate PDI activity.

The experiments performed in this study, highly suggest that lysine plays a critical role in PDI redox activity. The active site-flanking lysine residues play an important role for optimal substrate binding as well as for optimal turnover rate for the enzyme. The catalytic efficiency of wt-PDI discovered through our analysis was higher than previously reported (Raturi & Mutus, 2007). This study hints that acetylation may play a possible role in post-translational modification used by cells to regulate PDI activity. Further studies are required to fully understand how exactly acetylation may regulate PDI redox activity. However, in this report, it is suggested that acetylation may have activation and inhibitory effects on PDI redox activity. More investigation should be

performed on how different types of post-translational modifications regulate PDI activity, specifically on lysine residues. Notable post-translational modifications to investigate include methylation and succinylation.



## References

- Aka, J. A., Kim, G. W., & Yang, X. J. (2011). K-acetylation and its enzymes: overview and new developments. *Handb Exp Pharmacol*, 206, 1-12. doi: 10.1007/978-3-642-21631-2\_1
- Alanen, H. I., Salo, K. E., Pekkala, M., Siekkinen, H. M., Pirneskoski, A., & Ruddock, L. W. (2003). Defining the domain boundaries of the human protein disulfide isomerases. *Antioxid Redox Signal*, 5(4), 367-374. doi: 10.1089/152308603768295096
- Ali Khan, H., & Mutus, B. (2014). Protein disulfide isomerase a multifunctional protein with multiple physiological roles. *Front Chem*, 2, 70. doi: 10.3389/fchem.2014.00070
- Araki, K., Iemura, S., Kamiya, Y., Ron, D., Kato, K., Natsume, T., & Nagata, K. (2013). Ero1-alpha and PDIs constitute a hierarchical electron transfer network of endoplasmic reticulum oxidoreductases. *J Cell Biol*, 202(6), 861-874. doi: 10.1083/jcb.201303027
- Araki, K., & Nagata, K. (2011). Functional in vitro analysis of the ERO1 protein and protein-disulfide isomerase pathway. *J Biol Chem*, 286(37), 32705-32712. doi: 10.1074/jbc.M111.227181
- Bastos-Aristizabal, S., Kozlov, G., & Gehring, K. (2014). Structural insight into the dimerization of human protein disulfide isomerase. *Protein Sci*. doi: 10.1002/pro.2444
- Cai, H., Wang, C. C., & Tsou, C. L. (1994). Chaperone-like activity of protein disulfide isomerase in the refolding of a protein with no disulfide bonds. *J Biol Chem*, 269(40), 24550-24552.
- Cho, J. (2013). Protein disulfide isomerase in thrombosis and vascular inflammation. *J Thromb Haemost*. doi: 10.1111/jth.12413
- Denisov, A. Y., Maattanen, P., Dabrowski, C., Kozlov, G., Thomas, D. Y., & Gehring, K. (2009). Solution structure of the bb' domains of human protein disulfide isomerase. *FEBS J*, 276(5), 1440-1449. doi: 10.1111/j.1742-4658.2009.06884.x

- Dill, K. A., & MacCallum, J. L. (2012). The protein-folding problem, 50 years on. *Science*, 338(6110), 1042-1046. doi: 10.1126/science.1219021
- Dormeyer, W., Ott, M., & Schnolzer, M. (2005). Probing lysine acetylation in proteins: strategies, limitations, and pitfalls of in vitro acetyltransferase assays. *Mol Cell Proteomics*, 4(9), 1226-1239. doi: 10.1074/mcp.M500047-MCP200
- Edman, J. C., Ellis, L., Blacher, R. W., Roth, R. A., & Rutter, W. J. (1985). Sequence of protein disulphide isomerase and implications of its relationship to thioredoxin. *Nature*, 317(6034), 267-270.
- El Hindy, M., Hezwani, M., Corry, D., Hull, J., El Amraoui, F., Harris, M., . . . Conway, M. E. (2013). The Branched-Chain Aminotransferase Proteins: Novel Redox Chaperones for Protein Disulfide Isomerase-Implications in Alzheimer's Disease. *Antioxid Redox Signal*. doi: 10.1089/ars.2012.4869
- Flaumenhaft, R. (2013). Protein disulfide isomerase as an antithrombotic target. *Trends Cardiovasc Med*, 23(7), 264-268. doi: 10.1016/j.tcm.2013.03.001
- Freedman, R. B., Gane, P. J., Hawkins, H. C., Hlodan, R., McLaughlin, S. H., & Parry, J. W. (1998). Experimental and theoretical analyses of the domain architecture of mammalian protein disulphide-isomerase. *Biol Chem*, 379(3), 321-328.
- Fu, X. M., Wang, P., & Zhu, B. T. (2011). Characterization of the estradiol-binding site structure of human pancreas-specific protein disulfide isomerase: indispensable role of the hydrogen bond between His278 and the estradiol 3-hydroxyl group. *Biochemistry*, 50(1), 106-115. doi: 10.1021/bi101451g
- Goldberger, R. F., Epstein, C. J., & Anfinsen, C. B. (1963). Acceleration of reactivation of reduced bovine pancreatic ribonuclease by a microsomal system from rat liver. *J Biol Chem*, 238, 628-635.
- Goldberger, R. F., Epstein, C. J., & Anfinsen, C. B. (1964). Purification and Properties of a Microsomal Enzyme System Catalyzing the Reactivation of Reduced Ribonuclease and Lysozyme. *J Biol Chem*, 239, 1406-1410.
- Gupta, M. P., Samant, S. A., Smith, S. H., & Shroff, S. G. (2008). HDAC4 and PCAF bind to cardiac sarcomeres and play a role in regulating myofilament contractile activity. *J Biol Chem*, 283(15), 10135-10146. doi: 10.1074/jbc.M710277200

- Holmgren, A. (1968). Thioredoxin. 6. The amino acid sequence of the protein from *Escherichia coli* B. *Eur J Biochem*, 6(4), 475-484.
- Holmgren, A. (1979). Thioredoxin catalyzes the reduction of insulin disulfides by dithiothreitol and dihydrolipoamide. *J Biol Chem*, 254(19), 9627-9632.
- Karala, A. R., Lappi, A. K., & Ruddock, L. W. (2010). Modulation of an active-site cysteine pKa allows PDI to act as a catalyst of both disulfide bond formation and isomerization. *J Mol Biol*, 396(4), 883-892. doi: 10.1016/j.jmb.2009.12.014
- Kemmink, J., Darby, N. J., Dijkstra, K., Nilges, M., & Creighton, T. E. (1997). The folding catalyst protein disulfide isomerase is constructed of active and inactive thioredoxin modules. *Curr Biol*, 7(4), 239-245.
- Kimura, T., Nishida, A., Ohara, N., Yamagishi, D., Horibe, T., & Kikuchi, M. (2004). Functional analysis of the CXXC motif using phage antibodies that cross-react with protein disulphide-isomerase family proteins. *Biochem J*, 382(Pt 1), 169-176. doi: 10.1042/BJ20040116
- Koch, G. L. (1987). Reticuloplasmins: a novel group of proteins in the endoplasmic reticulum. *J Cell Sci*, 87 ( Pt 4), 491-492.
- Koivunen, P., Pirneskoski, A., Karvonen, P., Ljung, J., Helaakoski, T., Notbohm, H., & Kivirikko, K. I. (1999). The acidic C-terminal domain of protein disulfide isomerase is not critical for the enzyme subunit function or for the chaperone or disulfide isomerase activities of the polypeptide. *Embo Journal*, 18(1), 65-74. doi: 10.1093/emboj/18.1.65
- Kozarova, A., Sliskovic, I., Mutus, B., Simon, E. S., Andrews, P. C., & Vacratsis, P. O. (2007). Identification of redox sensitive thiols of protein disulfide isomerase using isotope coded affinity technology and mass spectrometry. *J Am Soc Mass Spectrom*, 18(2), 260-269. doi: 10.1016/j.jasms.2006.09.023
- Kozlov, G., Maattanen, P., Thomas, D. Y., & Gehring, K. (2010). A structural overview of the PDI family of proteins. *FEBS J*, 277(19), 3924-3936. doi: 10.1111/j.1742-4658.2010.07793.x
- Lee, K. K., & Workman, J. L. (2007). Histone acetyltransferase complexes: one size doesn't fit all. *Nat Rev Mol Cell Biol*, 8(4), 284-295. doi: 10.1038/nrm2145

- Li, H., Robertson, A. D., & Jensen, J. H. (2005). Very fast empirical prediction and rationalization of protein pKa values. *Proteins*, *61*(4), 704-721. doi: 10.1002/prot.20660
- Lyles, M. M., & Gilbert, H. F. (1991). Catalysis of the oxidative folding of ribonuclease A by protein disulfide isomerase: dependence of the rate on the composition of the redox buffer. *Biochemistry*, *30*(3), 613-619.
- Maattanen, P., Gehring, K., Bergeron, J. J., & Thomas, D. Y. (2010). Protein quality control in the ER: the recognition of misfolded proteins. *Semin Cell Dev Biol*, *21*(5), 500-511. doi: 10.1016/j.semcdb.2010.03.006
- Mamathambika, B. S., & Bardwell, J. C. (2008). Disulfide-linked protein folding pathways. *Annu Rev Cell Dev Biol*, *24*, 211-235. doi: 10.1146/annurev.cellbio.24.110707.175333
- Marcus, N., Shaffer, D., Farrar, P., & Green, M. (1996). Tissue distribution of three members of the murine protein disulfide isomerase (PDI) family. *Biochim Biophys Acta*, *1309*(3), 253-260.
- Marmorstein, R. (2001). Structure and function of histone acetyltransferases. *Cell Mol Life Sci*, *58*(5-6), 693-703.
- Marmorstein, R. (2004). Biochemical and structural characterization of recombinant histone acetyltransferase proteins. *Methods Enzymol*, *376*, 106-119. doi: 10.1016/S0076-6879(03)76007-8
- McLaughlin, S. H., & Bulleid, N. J. (1998). Thiol-independent interaction of protein disulphide isomerase with type X collagen during intra-cellular folding and assembly. *Biochem J*, *331* ( Pt 3), 793-800.
- Narayan, M. (2012). Disulfide bonds: protein folding and subcellular protein trafficking. *FEBS J*, *279*(13), 2272-2282. doi: 10.1111/j.1742-4658.2012.08636.x
- Nelson, J. W., & Creighton, T. E. (1994). Reactivity and ionization of the active site cysteine residues of DsbA, a protein required for disulfide bond formation in vivo. *Biochemistry*, *33*(19), 5974-5983.

- Noiva, R. (1999). Protein disulfide isomerase: the multifunctional redox chaperone of the endoplasmic reticulum. *Semin Cell Dev Biol*, 10(5), 481-493. doi: 10.1006/scdb.1999.0319
- Ogryzko, V. V., Schiltz, R. L., Russanova, V., Howard, B. H., & Nakatani, Y. (1996). The Transcriptional Coactivators p300 and CBP Are Histone Acetyltransferases. *Cell*, 87(5), 953-959. doi: [http://dx.doi.org/10.1016/S0092-8674\(00\)82001-2](http://dx.doi.org/10.1016/S0092-8674(00)82001-2)
- Onuchic, J. N., & Wolynes, P. G. (2004). Theory of protein folding. *Curr Opin Struct Biol*, 14(1), 70-75. doi: 10.1016/j.sbi.2004.01.009
- Patel, J., Pathak, R. R., & Mujtaba, S. (2011). The biology of lysine acetylation integrates transcriptional programming and metabolism. *Nutr Metab (Lond)*, 8, 12. doi: 10.1186/1743-7075-8-12
- Pehar, M., Lehnus, M., Karst, A., & Puglielli, L. (2012). Proteomic assessment shows that many endoplasmic reticulum (ER)-resident proteins are targeted by N(epsilon)-lysine acetylation in the lumen of the organelle and predicts broad biological impact. *J Biol Chem*, 287(27), 22436-22440. doi: 10.1074/jbc.C112.362871
- Pehar, M., & Puglielli, L. (2013). Lysine acetylation in the lumen of the ER: a novel and essential function under the control of the UPR. *Biochim Biophys Acta*, 1833(3), 686-697. doi: 10.1016/j.bbamcr.2012.12.004
- Ramachandran, N., Root, P., Jiang, X. M., Hogg, P. J., & Mutus, B. (2001). Mechanism of transfer of NO from extracellular S-nitrosothiols into the cytosol by cell-surface protein disulfide isomerase. *Proc Natl Acad Sci U S A*, 98(17), 9539-9544. doi: 10.1073/pnas.171180998
- Raturi, A., & Mutus, B. (2007). Characterization of redox state and reductase activity of protein disulfide isomerase under different redox environments using a sensitive fluorescent assay. *Free Radic Biol Med*, 43(1), 62-70. doi: 10.1016/j.freeradbiomed.2007.03.025
- Root, P., Sliskovic, I., & Mutus, B. (2004). Platelet cell-surface protein disulphide-isomerase mediated S-nitrosoglutathione consumption. *Biochem J*, 382(Pt 2), 575-580. doi: 10.1042/BJ20040759

- Sliskovic, I., Raturi, A., & Mutus, B. (2005). Characterization of the S-denitrosation activity of protein disulfide isomerase. *J Biol Chem*, *280*(10), 8733-8741. doi: 10.1074/jbc.M408080200
- Spange, S., Wagner, T., Heinzl, T., & Kramer, O. H. (2009). Acetylation of non-histone proteins modulates cellular signalling at multiple levels. *Int J Biochem Cell Biol*, *41*(1), 185-198. doi: 10.1016/j.biocel.2008.08.027
- Turano, C., Coppari, S., Altieri, F., & Ferraro, A. (2002). Proteins of the PDI family: unpredicted non-ER locations and functions. *Journal of Cellular Physiology*, *193*(2), 154-163. doi: 10.1002/jcp.10172
- Walker, K. W., & Gilbert, H. F. (1997). Scanning and escape during protein-disulfide isomerase-assisted protein folding. *J Biol Chem*, *272*(14), 8845-8848.
- Wang, C., Li, W., Ren, J., Fang, J., Ke, H., Gong, W., . . . Wang, C. C. (2013). Structural insights into the redox-regulated dynamic conformations of human protein disulfide isomerase. *Antioxid Redox Signal*, *19*(1), 36-45. doi: 10.1089/ars.2012.4630
- Wang, C., Yu, J., Huo, L., Wang, L., Feng, W., & Wang, C. C. (2012). Human protein-disulfide isomerase is a redox-regulated chaperone activated by oxidation of domain a'. *J Biol Chem*, *287*(2), 1139-1149. doi: 10.1074/jbc.M111.303149
- Wang, L., Wang, X., & Wang, C. C. (2015). Protein disulfide-isomerase, a folding catalyst and a redox-regulated chaperone. *Free Radic Biol Med*, *83*, 305-313. doi: 10.1016/j.freeradbiomed.2015.02.007
- Watanabe, M. M., Laurindo, F. R., & Fernandes, D. C. (2014). Methods of measuring protein disulfide isomerase activity: a critical overview. *Front Chem*, *2*, 73. doi: 10.3389/fchem.2014.00073
- Wilkinson, B., & Gilbert, H. F. (2004). Protein disulfide isomerase. *Biochim Biophys Acta*, *1699*(1-2), 35-44. doi: 10.1016/j.bbapap.2004.02.017
- Wu, M. M., Llopis, J., Adams, S., McCaffery, J. M., Kulomaa, M. S., Machen, T. E., . . . Tsien, R. Y. (2000). Organelle pH studies using targeted avidin and fluorescein-biotin. *Chem Biol*, *7*(3), 197-209.

Yoshimori, T., Semba, T., Takemoto, H., Akagi, S., Yamamoto, A., & Tashiro, Y. (1990). Protein disulfide-isomerase in rat exocrine pancreatic cells is exported from the endoplasmic reticulum despite possessing the retention signal. *J Biol Chem*, 265(26), 15984-15990.

Zhang, Z., Tan, M., Xie, Z., Dai, L., Chen, Y., & Zhao, Y. (2011). Identification of lysine succinylation as a new post-translational modification. *Nat Chem Biol*, 7(1), 58-63. doi: 10.1038/nchembio.495

## **Vita Auctoris**

NAME: Hyder Ali Khan

PLACE OF BIRTH Scarborough, Ontario

YEAR OF BIRTH 1991

EDUCATION Sandwich Secondary School, LaSalle, Ontario  
2005-2009

University of Windsor, Windsor, Ontario  
2009-2013 B.Sc. Honours Biochemistry with Thesis

University of Windsor, Windsor, Ontario  
2013-Present M.Sc. Biochemistry